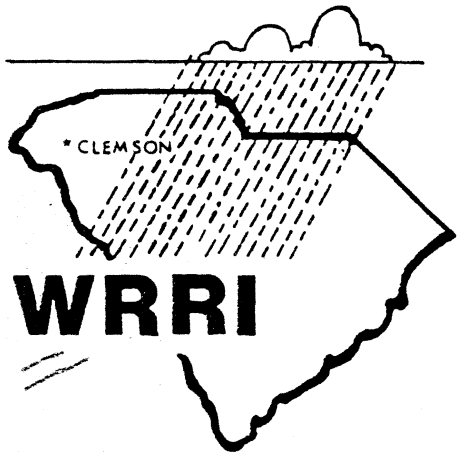

Report No. 124

CONTAMINANT TRANSPORT IN THE UNSTATURATED ZONE

by

Abbas A. Fiuzat
and
David Moughton
Civil Engineering Department
Clemson University
Clemson, SC 29634-0911

SOUTH CAROLINA
WATER RESOURCES RESEARCH INSTITUTE
Clemson, South Carolina
29634-2900

CLEMSON UNIVERSITY

May 1987

Technical Completion Report
G 1251-05

CONTAMINANT TRANSPORT IN THE UNSATURATED ZONE

by

Abbas A. Fiuzat and David Moughton
Department of Civil Engineering
Clemson University
Clemson, SC 29634

Submitted to:
United States Department of Interior
U.S. Geological Survey
Reston, VA 22092

The research on which this report is based was financed in part by the United States Department of the Interior, Geological Survey, through the South Carolina Water Resources Research Institute

South Carolina Water Resources Research Institute
Clemson University
Clemson, SC 29634-2900
May 1987

Project Agreement No. 14-08-0001-G1251
Period of Investigation: 5/1/86 - 4/30/87

ABSTRACT

The problem of flow in unsaturated soils is not fully understood. Several models of vertical flow in unsaturated soils exist and have been compared to laboratory data. This report compares four flow equations and five conductivity equations against each other and against a set of field data.

The equations compared were the flow equations of Darcy, Klute, Morel-Seytoux and Gelhar. The equations of hydraulic conductivity compared were those of Averjanov, Mualem, Irmay, Corey, and Laliberte, Brooks and Corey.

The equation combinations were compared by three different views, using both graphical and the root mean squares methods. First, a plot of the estimated time versus depth from the field study was compared with the equations' predictions. Next, nondimensional velocities were compared in graphs and by root mean squares. Presented last were graphic and numeric comparisons of the logs of the nondimensional velocities.

Based on the log root mean squares and the appropriateness of the derivation, Gelhar's equation of flow and Corey's equation of conductivity were chosen as agreeing most with the field data, though all equation combinations gave estimates ranging from an order of magnitude greater to an order of magnitude less than the field data.

TABLE OF CONTENTS

LIST OF FIGURES

LIST OF FIGURES CONTINUED

LIST OF TABLES

Chapter 1
INTRODUCTION

Flow through porous media is complex. Much more so is flow through media that are not saturated with the flowing fluid. Among the multitude of differences between flow through porous media and that in pipes and channels are the tortuosity of the flow path, pore size variation and distribution, particle size and shape, and fluid-particle interaction. In the case of unsaturated flow there is a second fluid involved, namely, air. Therefore capillary effects, surface tension, pressure gradients in the two fluids, and the degree of saturation all affect unsaturated flow. Before examining the flow equations, some background information about the terms and concepts used in unsaturated flow are useful.

The first step is to examine the porous medium through which the fluid passes. The medium consists of a collection of solid particles in contact, if not joined, and a series of spaces, or pores, between them. In the case of soils, a range of various sizes of soil particles make up the medium. The particles of soil are randomly distributed, creating a corresponding random range of pore sizes. The size range of the pores depends on the size and compaction of the particles. A finer grained or more tightly compacted soil has smaller pores. The fluid flows through the connecting necks between pores where the soil particles do not touch.

The properties of the particles affect the flow of the fluid. Some materials such as clay expand upon absorbing water. Expansion shrinks the size of the pores and may close off the connection between pores. Some soil particles such as clays have a surface charge that attracts water particles more strongly. This attraction increases the thickness of the residual water layer that remains on the particles when the medium is drained. Increasing the residual saturation decreases the available storage of the soil and also decreases the flow rate by decreasing the cross sectional area available for flow.

The properties of the flowing fluid have an effect on the flow. A more viscous fluid flows slower than a less viscous one. Especially important for unsaturated flow is the capillary effect. At the interface between two fluids and a surrounding solid, a meniscus forms. At the solid-liquid interface, the liquid contacts the solid at an angle particular to the solid-liquid combination. The liquid-air surface tension pulls the liquid-air interface into a three dimensional bowl, the meniscus, to connect the angled solid-liquid rim. In order to support the curve, there must be a pressure difference across the meniscus, known as capillary pressure. Without a pressure difference the liquid-air interface would be a flat surface, like a water-air interface on a lake. But in a porous medium the solid-liquid contact is at an angle so the liquid surface must be curved to keep a smooth surface. A way to visualize this is to picture a slender steel rod. Put the ends of the rod into clips on a horizontal track and allow the rod to hang horizontally. The clips and the track are arranged to hold the rod up but give no lateral support. To get the ends of the rod to form an angle to the track weights must be hung from the rod. The effect of weights on the steel rod is analogous to that of a pressure differential across the

liquid-air interface. In a soil the angle of solid-water contact is such that the meniscus forms concave into the water. To support the concavity, the water pressure must be less than the air pressure. The air is usually connected to the soil surface through a network of pores so the air is very close to atmospheric pressure even at great depths. The water, then, must be at a pressure less than atmospheric. At the water table, the water pressure is at atmospheric pressure because the water table surface is a free water surface, like a lake. Below the water table the water pressure is greater than atmospheric and increases with depth. To possess pressures less than atmospheric, the water must then be above the water table. The degree of curvature, hence the pressure difference, also depends on the size of the pore. A larger pore has a flatter meniscus so it has a smaller pressure difference than a smaller pore at the same elevation. Soils with smaller pores, from smaller particles or greater packing, can support interfaces with higher pressure differences. To reach a higher pressure difference, the water is supported at a higher elevation above the water table. The driving force exerted by the pressure difference is resisted by the solid-liquid attraction. The pressure difference does push the water deeper into the connection between the pores. The connections are narrower than the pores so the connections have a more curved meniscus and support a greater pressure difference.

The effects of pore size distribution, capillary pressure, and soil-water attraction can be observed in the drainage curve, shown in Figure 1-1. The drainage curve is the curve relating capillary pressure with water content or any other measure of the amount of water in the pores. The curve is made by allowing a saturated sample of soil to drain and measuring the water content and the capillary pressure as the soil drains. The result is an 'S' shaped curve. At saturation, the capillary pressure is zero. The capillary pressure increases without the water content decreasing, until some of the largest pores begin to drain, creating a short vertical line for the drainage curve. Drainage happens because the force of gravity creates a pressure difference greater than can be supported by the meniscus, determined by the pore diameter. Because of the pore size, the pressure difference is small. This pressure is the pressure at which drainage begins, or air first enters into the medium, and is important as a property of the soil. Petroleum engineers call this pressure the displacement pressure p_d; in the ceramics profession it is called the bubbling pressure p_b; and the soil scientists refer to it as the air-entry pressure p_e. As the drainage continues, the pores that are draining become smaller in size and more numerous. The smaller size causes a greater capillary pressure to overcome the more curved, and therefore stronger meniscuses. The line of the capillary pressure-water content assumes a constant slope of increasing capillary pressure and decreasing water content (Fig. 1-1). As this process continues, increasingly smaller (and less frequent) pores remain to be drained. The smaller pores can support a large pressure difference, and hence the curve steepens. As the pressure still increases, the last pores are drained and the connecting necks start to drain. The necks being smaller in both diameter and volume, the curve approaches a vertical asymptote. The asymptote is the line of residual saturation, which is the water content of the soil left at an infinite, or reasonably

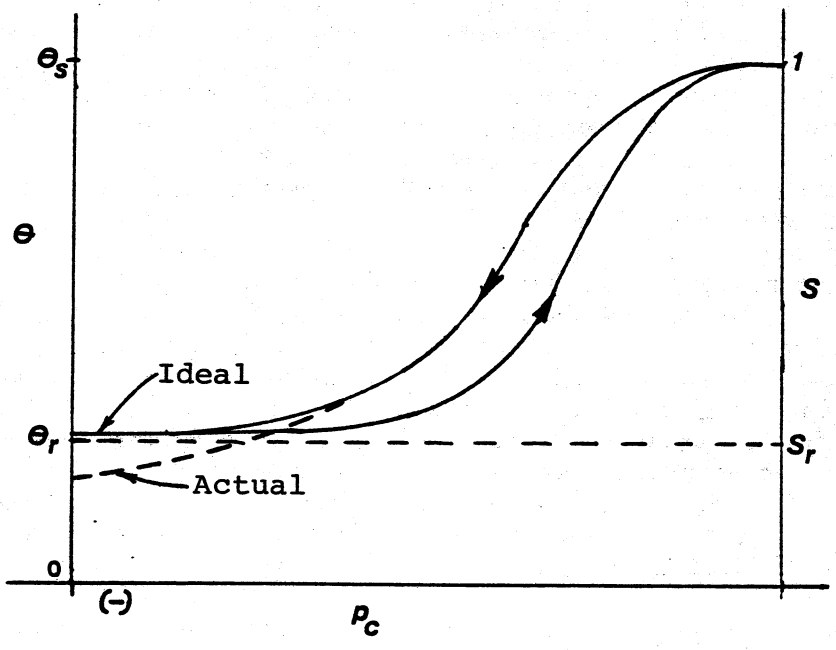

Fig. 1-1. A Typical Moisture Content Curve

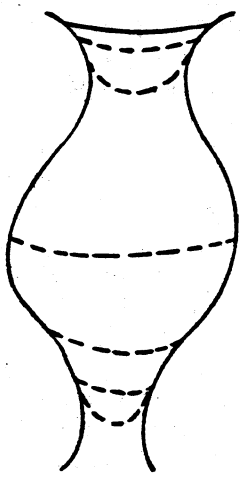

Fig. 1-2. Movement of Water Meniscus Through a Pore

molecular attraction. The more attractive the soil and the more surface area to contact the water, the higher the residual saturation. Clays, having small particles thus large surface areas and being more ionic than other soils, have the largest residual saturation.

Another aspect of the capillary pressure-water content curve is hysteresis. Consider the pore shown in Figure 1-2. When the pressure gradient is great enough to bring the meniscus down into the upper end of the pore, the widening of the pore diameter causes some changes in the movement of the meniscus. The outward angle of the pore walls cause the curvature of the meniscus to increase. The capillary pressure to drive the meniscus down increases. As the walls widen and approach parallel, the needed capillary pressure decreases. At some point the needed capillary pressure drops below the capillary pressure at the point and the pore suddenly drains completely. Refilling the pore has a different sequence. The meniscus is at the bottom of the pore. The capillary pressure is then decreased slightly to move the meniscus up into the pore. The widening of the pore causes a decrease in the curvature. To move the meniscus up the pore, the capillary pressure must decrease. At some point where the walls begin to narrow and approach parallel, the capillary pressure to support the meniscus rises above the capillary pressure at the point. Suddenly the pore fills. The pressure at which the pore suddenly drains and the pressure at which it suddenly fills occur at different points, neither of which is near the center of the pore height. The middle portion of the pore forms a difference in pore water volume of a graph of capillary pressure versus water content. The arrows in Figure 1-1 indicate the drainage versus wetting cycles of the curve.

The factors discussed above cause some of the major differences between flow in porous media and that of channels or pipes. The remainder of this report presents some of the unsaturated flow equations and discusses their performance in relation to a set of existing data on unsaturated flow in soils.

Chapter 2

EXPLANATION OF UNSATURATED FLOW TERMS

In this part of the report some of the basic concepts and definitions associated with flow through unsaturated soils are reviewed. The first terms to understand are those dealing with the amount of water or air in the soil matrix. Flow in the soil is highly dependent on the amount of water in the soil, not for the mass in flow, but for the effects of water content on the flow characteristics.

Water content θ is a measure of the amount of water in the soil. The water content is defined as the volume of water per unit volume of soil. This property is a measure of the absolute amount of water.

Porosity ϕ is the total volume of pores or voids in a unit volume of soil. The pores include those filled with water and those with both air and water.

Saturation S is the fraction of the pore volume filled with water. Saturation is equal to the ratio of water content over the porosity. Equivalently, it is the volume of water per unit of pore volume.

The residual saturation Sr is the fraction of pore volume that is taken up by water adsorbed so tightly to the soil particles that no pressure gradient can remove it. This moisture can be detached from the soil by other means such as heating a soil sample in the oven, but field gradients would not be able to deplete the soil of this residual water content.

The effective saturation Se is the ratio of the volume of drainable water over the non-residual pore volume:

$$Se = \frac{(S - Sr)}{(1 - Sr)} \qquad (2\text{-}1)$$

The energy per unit weight of the moving fluid is called head, measured in depth of water. Total head H includes the potential energy due to elevation, pressure of the fluid and the kinetic energy of the moving fluid. In movement of water through soils, however, velocities are usually very small and the kinetic energy is often negligible, much more so in the case of unsaturated flow.

The hydraulic conductivity K is the rate of movement of a fluid through the soil under a unit gradient of head. The hydraulic conductivity (units $\equiv$ V) is a function of both the soil matrix and the properties of the flowing fluid. It is preferable, however, to define a term for the ease of flow through soils that is only dependent on the soil itself, and not on the moving fluid. This term is called the intrinsic permeability, or simply permeability k, and is measured in units of L^2. Saturated conductivity is directly related to permeability by the following equation:

$$K = \frac{k\ \rho\ g}{\mu} \qquad (2\text{-}2)$$

where k is the permeability in units of area, ρ is the fluid density in mass per volume, g is the acceleration of gravity in length per time squared and μ is the fluid dynamic viscosity in force-time per area.

The pore size distribution is quantified by an index λ, which increases as the size range of the pores decreases. Higher volumes of λ correspond to coarser, more thoroughly mixed, more densely packed or more uniformly sized soils. To determine λ, a plot of p_c vs S or Se is needed. If substantial data for plotting of such a relationship is available, λ is found from the following equation:

$$\lambda = \frac{1/N\ [\Sigma\ (\log p_c)]\ [\Sigma\ (\log Se)] - \Sigma\ (\log p_c\ \log Se)}{\Sigma\ [(\log p_c)^2] - 1/N\ [\Sigma(\log p_c)]^2} \qquad (2\text{-}3)$$

and

$$p_b = \text{antilog}\ \{\ 1/N\ [\Sigma(\log p_c) + 1/\lambda\ \Sigma(\log Se)]\ \} \qquad (2\text{-}4)$$

On the other hand, if only a few data points for p_c vs S or Se are available, λ is found by curve-fitting to the data using the following relationship:

$$S = (1 - Sr)\ (p_b/p_c)^{\lambda} + Sr \qquad (2\text{-}5)$$

Using Eq. 2-1, Eq. 2-5 can be converted to:

$$Se = (p_b/p_c)^{\lambda} \qquad (2\text{-}6)$$

In this case p_b should be found or estimated. For this report a computer program was developed to examine all possible values of p_b, λ and Sr in order to find the best fit for the available data of S vs p_c.

Chapter 3

LITERATURE SEARCH

The starting point in the search for equations for the velocity and the hydraulic conductivity was a computer literature search. The first database searched was the National Technical Information Service (NTIS). This database contains a listing of all the research done for or by a federal government agency. The next database searched was the Engineering Database (ENGI1). ENGI1 contains the articles printed in a variety of technical journals in the different engineering fields. The third database searched was the Agricultural Library (ARGRICOLA). Articles from agricultural journals are listed in this database.

From the listings given by the computer search, four equations of fluid flow in unsaturated soils were chosen. These equations were those of Darcy, Klute, Morel-Seytoux, and Gelhar as given below. The primary criterion for the selection of these equations was their requirement of data that are normally collected in a survey. Since this comparison would be conducted with data collected in the field, all equations had to be satisfied using the available data. Each equation requires the knowledge of a relationship between moisture content and the hydraulic conductivity. Several equations defining this relationship exist, from which four were chosen for the purposes of this study and will be reviewed in the next chapter. Thus, a total of eight equations were used. The selected equations for flow velocity through unsaturated soils are explained below.

DARCY

The first equation of motion is Darcy's law of fluid motion. Darcy [cited in Corey, 1977] stated that the flow velocity through porous media is equal to the product of the total head gradient times the hydraulic conductivity of the soil and fluid:

$$v_w = K \nabla H \tag{3-1}$$

Darcy's law was proven experimentally for saturated soils and found to be accurate. The equation was extended to unsaturated soils and assumed to work with the proper K function.

MOREL-SEYTOUX

Morel-Seytoux (1973) based his equation on Darcy's law. Morel-Seytoux combined two Darcy equations, one for the water flow and one for the air flow. He started with the basic vertical flow equation:

$$v_i = \frac{-k\, k_{ri}}{\mu_i} \frac{dp_i}{dz} + \frac{k k_{ri}}{\mu_i} \rho_i g \tag{3-2}$$

where v_i is the macroscopic fluid velocity in length per time, k is the permeability of the soil in length squared, k_{ri} is the relative permeability, the actual permeability of the soil at the present saturation over the saturated permeability, and is unitless, μ is the fluid viscosity in force by time over area, dp_i/dz is the pressure gradient of the fluid in force per area per length, ρ_i is the density of the fluid in mass per volume and g is the acceleration of gravity in length per time squared.

The equations for water and air are then:

$$v_w = \frac{-k\ k_{rw}}{\mu_w} \frac{dp_w}{dz} + \frac{k\ k_{rw}}{\mu_w} \rho_w g \tag{3-3}$$

$$v_a = \frac{-k\ k_{ra}}{\mu_a} \frac{dp_a}{dz} + \frac{k\ k_{ra}}{\mu_a} \rho_a g \tag{3-4}$$

where w is the subscript for water and a is the subscript for air.

Multiplying the water equation by μ_w/kk_{rw} and the air equation by $-\mu_a/kk_{rw}$ and then adding the resulting equations together:

$$\frac{\mu_w\ v_w}{k\ k_{rw}} - \frac{\mu_a\ v_a}{k\ k_{ra}} = \frac{dp_a}{dz} - \frac{dp_w}{dz} + g\ (\rho_w - \rho_a) \tag{3-5}$$

If the total volumetric flow of both fluids is Q then:

$$Q = Q_a + Q_w \tag{3-6}$$

where Q_a is the air flow and Q_w is the water flow. If A is the cross sectional area of the flow, then:

$$vA = (v_a + v_w)\ A \tag{3-7}$$

$$Q/A = v = v_a + v_w \tag{3-8}$$

where v is the total velocity of all the fluids.

The water fractional velocity, the water velocity's percentage of the total velocity is:

$$F = \frac{v_w}{v} \tag{3-9}$$

Introducing Eqs. 3-8 and 3-9 into Eq. 3-5 gives:

$$\frac{\mu_w vF}{k\ k_{rw}} - \frac{\mu_a v(1-F)}{k\ k_{ra}} = \frac{dp_a}{dz} - \frac{dp_w}{dz} + g\ (\rho_w - \rho_a) \tag{3-10}$$

The capillary pressure p_c is the difference between the air and the water pressures:

$$p_c = p_a - p_w \tag{3-11}$$

Using Eq. 3-11 in Eq. 3-10, we get:

$$\frac{\mu_w v F}{k\, k_{rw}} - \frac{\mu_a v(1-F)}{k\, k_{ra}} = \frac{dp_c}{dz} + g\,\Delta\rho \tag{3-12}$$

Moving v to the right side of the equation:

$$\frac{\mu_w F}{k\, k_{rw}} - \frac{\mu_a (1-F)}{k\, k_{ra}} = \frac{1}{v}\left(\frac{dp_c}{dz} + g\,\Delta\rho\right) \tag{3-13}$$

Multiplying through by kk_{ra}/μ_a:

$$\frac{\mu_w}{\mu_a}\frac{k_{ra}}{k_{rw}} F - 1 + F = \frac{k\, k_{ra}}{\mu_a v}\left(\frac{dp_c}{dz} + g\,\Delta\rho\right) \tag{3-14}$$

Adding 1 to both sides:

$$\left(\frac{\mu_w}{\mu_a}\frac{k_{ra}}{k_{rw}} + 1\right) F = 1 + \frac{k\, k_{ra}}{\mu_a v}\left(\frac{dp_c}{dz} + g\,\Delta\rho\right) \tag{3-15}$$

A variable f_w, a function of the permeabilities, is defined as:

$$f_w = \left(1 + \frac{\mu_w}{\mu_a}\frac{k_{ra}}{k_{rw}}\right)^{-1} \tag{3-16}$$

Using Eq. 3-16 in Eq. 3-15 gives:

$$\frac{F}{f_w} = 1 + \frac{k\, k_{ra}}{\mu_a v}\left(\frac{dp_c}{dz} + g\,\Delta\rho\right) \tag{3-17}$$

$$F = \left(\frac{v - v_a}{v}\right) = f_w\left(1 + \frac{k\, k_{ra}}{\mu_a v}\left(\frac{dp_c}{dz} + g\,\Delta\rho\right)\right) \tag{3-18}$$

$$1 - \frac{v_a}{v} = f_w\left(1 + \frac{k\, k_{ra}}{\mu_a v}\left(\frac{dp_c}{dz} + g\,\Delta\rho\right)\right) \tag{3-19}$$

$$1 - f_w = \frac{v_a}{v} + \frac{f_w k\, k_{ra}}{\mu_a v}\left(\frac{dp_c}{dz} + g\,\Delta\rho\right) \tag{3-20}$$

$$v(1 - f_w) = v_a + \frac{f_w\ k\ k_{ra}}{\mu_a} \left(\frac{dp_c}{dz} + g\ \Delta\rho\right) \tag{3-21}$$

$$v(1 - f_w) = \frac{-k\ k_{ra}}{\mu_a} \frac{dp_a}{dz} + \frac{k\ k_{ra}}{\mu_a} \rho_a g + \frac{f_w k\ k_{ra}}{\mu_a} \left(\frac{dp_c}{dz} + g\ \Delta\rho\right) \tag{3-22}$$

Dividing through by kk_{ra}/μ_a:

$$\frac{\mu_a v\ (1-f_w)}{k\ k_{ra}} = \frac{-dp_a}{dz} + \rho_a g + f_w\left(\frac{dp_c}{dz} + g\ \Delta\rho\right) \tag{3-23}$$

The left side of Eq. 3-23 is simplified by:

$$\frac{(1-f_w)}{(k\ k_{ra}/\mu_a} = \frac{\mu_a}{k\ k_{ra}} \left(1 - \frac{1}{(1 + \mu_w/\mu_a\ k_{ra}/k_{rw})}\right)$$

$$= \frac{\mu_a}{k\ k_{ra}} \frac{([1 + \mu_w/\mu_a\ k_{ra}/k_{rw}] - 1)}{(1 + \mu_w/\mu_a\ k_{ra}/k_{rw})}$$

$$= \frac{\mu_a}{k\ k_{ra}} \frac{(\mu_w/\mu_a\ k_{ra}/k_{rw})}{(1 + \mu_w/\mu_a\ k_{ra}/k_{rw})}$$

$$= \frac{1}{k} \frac{\mu_w}{k_{rw}} \frac{1}{(1 + \mu_w/\mu_a\ k_{ra}/k_{rw})}$$

$$= \frac{1}{k} \frac{1}{(k_{rw}/\mu_w)} \frac{1}{(1 + \mu_w/\mu_a\ k_{ra}/k_{rw})}$$

$$= \frac{1}{k} \frac{1}{(k_{rw}/\mu_w + k_{ra}/\mu_a)}$$

Substituting the end result into Eq. 3-23:

$$\frac{v}{k} \frac{1}{(k_{rw}/\mu_w + k_{ra}/\mu_a)} = \frac{-dp_a}{dz} + \rho_a g + f_w\left(\frac{dp_c}{dz} + g\Delta\rho\right) \tag{3-24}$$

$$v = \left(k\left[\frac{kr_w}{\mu_w} + \frac{kr_a}{\mu_a}\right]\right) \left(\frac{-dp_a}{dz} + \rho_a g + f_w\left[\frac{dp_c}{dz} + g\ \Delta\rho\right]\right) \tag{3-25}$$

To find v_w:

$$v_w = vF = v \{f_w(1 + \frac{k\, k_{ra}}{\mu_a} [\frac{dp_c}{dz} + g\, \Delta\rho])\} \quad (3\text{-}26)$$

with

$$f_w = (1 + \frac{\mu_w}{\mu_a} \frac{k_{ra}}{k_{rw}})^{-1}$$

Note that

$$\frac{\Delta\theta}{\Delta t} = \frac{\Delta V_w}{V_t \Delta t} = \frac{\Delta z A}{LA\Delta t} = \frac{\Delta z/\Delta t}{L} = \frac{v_w}{L} \quad (3\text{-}27)$$

Morel-Seytoux's equation requires only the physical constants μ, ρ and z and the standard saturation vs pore pressure curves for k, k_{ri}, and P_c.

The Morel-Seytoux equation takes into account the fact that air must flow out of the media as the water flows in. The outflow of air is a major limiting factor in flow into enclosed volumes of porous media. The air will be trapped in the media and create a pressure gradient strong enough to counteract gravity and eliminate the capillary pressure gradient.

KLUTE

Klute's equation (1969) is based on both Darcy's law and conservation of mass. The conservation of mass is written as a flow equation:

$$F = J_l + J_v + C_l Q_l + C_v Q_v \quad (3\text{-}28)$$

where F is the total mass flow in mass per time, J is the diffusion of fluid in mass per time, C is the concentration of fluid in mass per volume, and Q is the volumetric flow rate of fluid in volume per time with l and v being the subscripts for liquid and vapor respectively.

Klute assumes that the mass flow due to diffusion is negligible. If the soil is relatively isothermal, as in deeper soils, there is no temperature gradient to drive the diffusion. If the soil is relatively moist then the gas is discontinuous and there is no path for the vapor to flow through.

Klute assumes that the gas flow can be ignored because the air has 1/50th the viscosity and 1/1000th the density of water. The air flow does not impede the water flow.

Taking the assumptions into account, Eq. 3-28 becomes:

$$F = C_l Q_l \quad (3\text{-}29)$$

The mass flow of water can also be written as:

$$d\rho_w/dt = F \tag{3-30}$$

with ρ_w as the mass of water in a unit volume of the soil, F is the mass flow and refers to the flow along all three axes. Then:

$$d\rho_w/dt = C_1 Q_1 \tag{3-31}$$

From Darcy's law (Eq. 3-1):

$$d\rho_w/dt = C_1 \nabla \cdot (K(\theta) \nabla H) \tag{3-32}$$

with K being the conductivity of the soil in length per time at volumetric water content θ in volume of water per volume of soil, ∇H is the total head gradient along all three axes and the symbol ∇ in front refers to the flow in all three directions.

The mass flow into a unit volume of soil can be referred to as:

$$d\rho_w/dt = C_1 \, d\theta/dt \tag{3-33}$$

the change in mass per unit volume of soil equals the change in the volume of water in the soil times the unit mass of water.

Equations 3-32 and 3-33 are equal:

$$C_1 \, d\theta/dt = C_1 \nabla \cdot (K(\theta) \nabla H) \tag{3-34}$$

$$d\theta/dt = \nabla \cdot (K(\theta) \nabla H) \tag{3-35}$$

The total head is the sum of capillary head h_c, the velocity head and the position head z. The velocities in unsaturated flow are so small as to be negligible.

$$d\theta/dt = \nabla \cdot (K(\theta) \nabla (h_c + z)) \tag{3-36}$$

To find the water velocity, the left side of Eq. 3-36 must be manipulated in a manner similar to Eq. 3-27:

$$\frac{d\theta}{dt} = \frac{dV_w}{Vdt} = \frac{Adz}{ALdt} = \frac{1}{L} \frac{dz}{dt} = \frac{v_w}{L} \tag{3-37}$$

where V and v denote volume and velocity, respectively, and V_w is the change in the volume of water per volume of soil, V_t is the total volume of soil, dt is the change in time, dz is the change in hydraulic head in units of length, A is the cross-section area of the volume of soil, L is the height of the soil volume in units of length.

Now v_w is given by:

$$v_w = L\nabla(K(\theta) \nabla (h_c + z)) \tag{3-38}$$

The flow is assumed to be downward only. This assumption is based on the idea that the changes in the water content brought on by the flow are constant across the horizontal cross section of soil.

$$v_w = L\nabla(K(\theta) (dh_c/dz + dz/dz)) \quad (3\text{-}39)$$

$$v_w = L\nabla(K(\theta) (dh_c/dz + 1)) \quad (3\text{-}40)$$

$$v_w = L\nabla[dK(\theta)/dz (dh_c/dz + 1) + K(\theta) (d^2h_c/dz^2)] \quad (3\text{-}41)$$

GELHAR

The volumetric flow Q of water is the effective velocity v through the cross sectional area A_t:

$$Q = v A_t \quad (3\text{-}43)$$

or

$$v = \frac{Q}{A_t} = q \quad (3\text{-}44)$$

where q is the volumetric flow through a unit area.

In an unsaturated porous media, the total cross sectional area is divided into three subareas; the solid area A_s, the water area A_w, and the air area A_a. Since the flow of water takes place only through the water area A_w and q is the flow through the total area A_t, v is actually:

$$v_w = \frac{Q}{A_t}\frac{A_t}{A_w} = \frac{qA_t}{A_w} \quad (3\text{-}45)$$

Assuming the porous media is isotropic:

$$\frac{A_w}{A_t} = \frac{V_w}{V_t} = \theta \quad (3\text{-}46)$$

where V_w is the volume of water in the total volume of soil V_t and θ is the soil water content.

Substituting Eq. 3-46 into Eq. 3-45 gives:

$$v = \frac{q}{\theta} \quad (3\text{-}47)$$

Gelhar (1974) experimentally determined that for a soil drained by gravity (where hydraulic gradient is unity and $dh_c/dz = 0$):

$$q = K \quad (3\text{-}48)$$

where K is the soil hydraulic conductivity at the given saturation. Therefore, for gravity drained soils:

$$v = \frac{K}{\theta} \tag{3-49}$$

Chapter 4

CONDUCTIVITY EQUATIONS

BASE EQUATION

This section deals with the equations that calculate the permeability or the hydraulic conductivity of the unsaturated soil for use in the flow equations that were given in Chapter 3. The equations used in this report are those derived by different authors, but are all based on the same basic equation. In this report, the simpler derivation of Brooks and Corey will be briefly presented, but equations of Averjanov, Corey, Irmay, Mualem, and Laliberte, Brooks and Corey will be used. Those equations are presented in the remainder of this chapter. For details of the derivations, the reader is referred to the original articles.

For a meniscus to be stable, there must be a balance of forces. The pressure difference p_c across the meniscus applied over the projected area of the meniscus dA is countered by the surface tension σ pulling on the soil at angle α around the wetted perimeter dwp:

$$p_c dA = \sigma \cos \alpha \, dwp \tag{4-1}$$

The hydraulic radius R of the meniscus is:

$$R = dA / dwp = \sigma \cos \alpha / (p_c) \tag{4-2}$$

p_c is a function of the saturation S. The average of the square of the hydraulic radius is:

$$R^2 = \frac{\sigma^2 \cos^2 \alpha}{S} \int_0^S \frac{dS}{p_c^2} \tag{4-3}$$

The Navier-Stokes equation for flow is:

$$u = \frac{R^2}{k_f \mu} \nabla p \tag{4-4}$$

with u the average macroscopic velocity in length per time, R is the hydraulic radius in length, k_f is the shape factor, a constant accounting for the shape of the flow cross section effecting the velocity, μ is the fluid viscosity in force-time per area and ∇p is the pressure gradient.

In porous media the flow does not follow a straight path. The fluid particle actually travels a tortuous distance Le in order to travel the macroscopic straight distance L so the actual velocity of the particle is:

$$v = u \, (Le/L) \tag{4-5}$$

with v the microscopic velocity.

The flow is powered by the driving gradient ∇p, which is simplified for flow in one direction, as:

$$\nabla p = \Delta p \ (L/Le) \tag{4-6}$$

Using Eqs. 4-5 and 4-6 in Eq. 4-4 gives:

$$v = \frac{R^2}{k_f \mu (Le/L)} \Delta p \frac{L}{Le} \tag{4-7}$$

$$v = \frac{R^2}{k_f \mu (Le/L)^2} \Delta p \tag{4-8}$$

The dimensionless term $(Le/L)^2$ accounts for the actual distance the flow has to travel. The term is generally called the tortuosity T. The fluid flows through the pores and around the soil particles at full saturation. As the saturation decreases and the pores begin to drain, the fluid must flow through fewer and fewer pores. The flow path begins to wind as the flow seeks the still connected pores. The microscopic flow travels at greater and greater angles to the macroscopic flow. The lower the saturation the more convoluted the path and the higher the tortuosity. The tortuosity has been experimentally determined to be related to the saturation by:

$$T_o/T = [(S-Sr)/(1-Sr)]^2 = Se^2 \tag{4-9}$$

where T_o is the tortuosity at full saturation, T is the tortuosity at the given saturation S, Sr is the residual saturation, Se is the effective saturation and 1 is the value of S at full saturation.

At full saturation, the instantaneous flow is assumed to be averaging a 45° angle to the macroscopic flow. If L is said to be 1 then Le is $\sqrt{2}/2$ and T_o is 2. Substituting Eq. 4-9 into Eq. 4-8 gives:

$$v = \frac{R^2}{k_f \mu T} \nabla P = \frac{R^2 Se^2}{2 k_f \mu} \Delta p \tag{4-10}$$

Using Eq. 4-3:

$$v = \frac{Se \ \sigma^2 \cos^2 \alpha}{2 k_f \mu} \Delta p \int_0^{Se} \frac{dSe}{(p_c)^2} \tag{4-11}$$

In 1863 Dupuit found that:

$$Q = v \phi_e \ Se \tag{4-12}$$

with ϕ_e as the effective porosity after accounting for the residual saturation and Q is the volumetric flow rate. From Darcy's law:

$$Q = K \Delta p \tag{4-13}$$

Setting Eqs. 4-12 and 4-13 equal:

$$K \Delta p = v\phi_e \, Se \tag{4-14}$$

Substituting Eq. 4-11 into Eq. 4-14:

$$K \Delta p = \frac{\phi_e \, Se^2 \, \sigma^2 \cos^2\alpha}{2 \, k_f \mu} \nabla p \int_0^{Se} \frac{dSe}{(p_c)^2} \tag{4-15}$$

$$K = \frac{\phi_e \, Se^2 \, \sigma^2 \cos^2\alpha}{2 \, k_f \, \mu} \int_0^{Se} \frac{dSe}{(p_c)^2} \tag{4-16}$$

In a fully saturated media, Se is 1, thus:

$$K_o = \frac{\phi_e \sigma^2 \cos^2\alpha}{2 \, k_f \, \mu} \int_0^{1} \frac{dSe}{(p_c)^2} \tag{4-17}$$

where K_o is the conductivity of the fully saturated media and K is the total conductivity of the soil at effective saturation Se, given by:

$$K = \frac{K_o \int_0^{Se} \frac{dSe}{(p_c)^2}}{\int_0^{1} \frac{dSe}{(p_c)^2}}$$

for K_o experimentally determined from soil samples.

In order to make Eq. 4-18 easier to use, simplifications have been devised to replace the integral terms in the equations. Corey (1954) experimentally determined that:

$$K = K_o Se^4 \tag{4-19}$$

Averjanov (1950) theoretically found that:

$$K = K_o Se^{3.5} \tag{4-20}$$

Irmay (1954) used a theoretical perfectly uniform pore size distribution to find:

$$K = K_o Se^3 \tag{4-21}$$

LALIBERTE, BROOKS and COREY

Brooks and Corey (1966) used the following equation:

$$K = \frac{\phi_e \, Se^2 \, \sigma^2 \, \cos^2\alpha}{2 \, k_f \, \mu} \int_0^{Se} \frac{dSe}{(p_c)^2} \qquad (4\text{-}16)$$

Laliberte, Brooks, and Corey (1968) said that $\cos^2 \alpha$ is assumed to be 1 for any α close to 0°. k_f is equal to 2 for a circular cross section and 3 for a thin film. For a porous media a value of 2.5 is assumed to account for the variety of shapes within pores and between pores. Equation 4-16 becomes:

$$K = \frac{\phi_e Se^2 \, \sigma^2}{5\mu} \int_0^{Se} \frac{dSe}{(p_c)^2} \qquad (4\text{-}22)$$

Brooks and Corey found that the effective saturation Se and the capillary pressure p_c are related by:

$$Se = (p_b/p_c)^{\lambda} \qquad (4\text{-}23)$$

where p_b is the bubbling pressure and the minimum p_c at which the air is continuous, and λ is the pore size distribution index. λ was defined by Brooks and Corey as the slope of the straight plot of logSe vs $\log(p_b/p_c)$. λ decreases as the number of different pore sizes increases. Substituting Eq. 4-23 into Eq. 4-22 gives:

$$K = \frac{\phi_e \, Se^2}{5\mu p_b^{\,2}} \int_0^{Se} \frac{Se^{(2/\lambda)}}{\lambda} \, dSe \qquad (4\text{-}24)$$

Setting the limits of integration as 0 and 1 for fully saturated soils:

$$K_o = \frac{\phi_e \, \sigma^2}{5\mu p_b^{\,2}} \quad \frac{1}{2\lambda+1} \quad Se^{(2\lambda+1)} \qquad (4\text{-}25)$$

$$K_o = \frac{\phi_e \, \sigma^2}{5\mu p_b^{\,2}} \quad \frac{\lambda}{\lambda+2} \qquad (4\text{-}26)$$

and

$$K = K_o \, (p_b/p_c)(2 + 3\lambda) \qquad (4\text{-}27)$$

where n is related to one or more properties of the specific soil. Mualem based n on the capillary pressure p_c vs water content θ curve because that curve is generally found in the normal course of a soil investigation. From this curve Mualem defined the term work w as the energy required to drain a soil from full saturation to complete drainage:

$$w = \gamma_w \int_{h_c = 0}^{h_c = \infty} h_c d\theta \qquad (4\text{-}29)$$

where γ_w is the specific weight of water in force per volume. Because the p_c vs θ curve is believed to show the effects of several soil characteristics, p_b, λ, etc., the exponent n should be related to w by some function. Mualem sought a function that met actual data, produced small errors between calculated n and data back-calculated n, and was simple. Mualem used the basic equation:

$$n = aw^{\alpha} + b \qquad (4\text{-}30)$$

with a, α and b empirical constants experimentally determined. By using the data from 50 different soil samples, Mualem found that $\alpha = 1$ and:

$$n = 0.015\ w + 3.0 \qquad (4\text{-}31)$$

fit the data well and met Averjanov's value for perfectly uniform pore size distributions.
1919

Chapter 5

THE FIELD DATA

COLLECTION OF DATA

To find the best equation for velocity and conductivity, field data had to be utilized on which to base the comparison. It was fortunate that certain field data were available, reported by Ligon and Wilson (1972) and Ligon et al (1980) of Clemson University's Department of Agricultural Engineering. The data consisted of a tritium tracer study on a plot in the Clemson research watershed. It would have been ideal to have more thorough field data, but given the total one-year duration of the study, acquisition of additional field data was not possible.

In the field study a slug of tritium was inserted in the surface layers of the soil column. At certain time intervals a series of soil samples were taken at specific depths. From the samples, radiation counts were taken to determine the radioactivity of the water at the sample depth at the sampling time. These counts were compared with background counts taken at such places as Lake Hartwell and a stream near the sample site. The data used in the present study were those of the deeper layers of soil where the moisture changes were smaller and the times between samples were larger. These conditions tend to cut down on variations in the flow.

The leading edge of the tritium trace was found by calculating the point where the sample counts dropped down to the background counts, a straight line interpolation was used to find the depth of the leading edge. The primary reasons why the leading edge of the tritium movement front was used instead of the point of peak concentration are the following: 1) The molecular structure and hence the potential of tritium for diffusion in a partially saturated soil is so close to water that the velocity of the moving front cannot be appreciably different than the velocity of point of peak tritium content; 2) the precision of the field data is not high enough to distinguish between these two velocities; and 3) since the application of the results of the study is in movement of contaminants through unsaturated soil, it is important to determine the location of the leading edge of a contaminant at any one time, rather than the point of highest concentration.

The velocity through a layer of soil was assumed to be the distance traveled by the tracer between sample times divided by the corresponding time interval. The velocity was assumed to be constant over the depth interval. Also taken during the field study were a number of measurements of the soil conditions. This information was needed for the comparison. The capillary pressure of the soil vs water content was taken for the values of 0 psi (full saturation), 1.5 psi, 4.9 psi, 9.9 psi, and 14.7 psi at each of the main data soil layers. The saturated hydraulic conductivity was taken for a different but corresponding series of soil layers. During another study in the same site, a number of soil moisture profiles were taken over a period of time from April 1970 to April 1971.

USE OF DATA AND EQUATIONS

The first step in the use of the data collected by Ligon et al was the generation of the type of data needed by the equations of conductivity and flow. The explanation of data manipulation described below is for one of the soil layers. The method is repeated for each of the other layers.

The first type of data generated were curves of capillary pressure p_c vs saturation S. The collected data were in the form of capillary pressure p_c vs water content θ at four different points. With the water content known, saturation can be found from the basic relation:

$$\theta = \phi S \qquad (5\text{-}1)$$

The saturation S at 0 psi is the full saturation of S = 1 at which point the value of water content θ is the same as the soil porosity ϕ. The water contents at each of the three remaining pressures were then divided by the porosity ϕ to give the saturation S at each pressure. These S vs p_c data were fed into a computer program to find the values of Sr, λ, and p_b found in Eq. 5-2. The computer program was developed specifically for this purpose and can be obtained from the authors.

$$S = (1 - Sr)\ (p_b/p_c)\lambda + Sr \qquad (5\text{-}2)$$

Starting with a set of values of p_b, Sr, and λ, the program calculated a series of trial S's for the set of p_c's. If the series of S's was quite close to the S's from the data set, the program would print out the trial S's, and the trial values of p_b, Sr, and λ. Using a nested set of loops the program would test all possible combinations of p_b, Sr, and λ. The printout of the trial S's would then be compared to the data S's to find the series that came the closest to the data. Frequently, the trial S's of a given set of values of p_b, Sr, and λ would match exactly for some of the data S's but not all. As a way to decide, the S's of the lower p_c's were given more weight than the higher p_c's. The primary reason for this method was that frequently some of the values of Sr were above the values of S given for higher p_c's and there would be no other comparison between the different sets of values of p_b, Sr, and λ. Also, small changes in the values of p_b, Sr and λ caused small changes in the trial S's at lower p_c's but large changes in the S's for higher p_c's.

After using the program to find the best values of p_b, Sr and λ, the S vs p_c curve was plotted with a vertical line at S = 1 up to p_b and an asymptote at Sr. The work w used in Mualem's equation of conductivity was found by determining the area under the curve.

The saturated conductivity K_o was found from the data given by Ligon et al. The data were taken in layers that were smaller and offset from the main data layers used for the S vs p_c curve and other information. Therefore the saturated conductivities for the main data layers were found by determining weighted average conductivities of the offset layers. The amount of each offset layer within the main layer determined the extent to which the offset layer affected the main layer.

In addition to the saturated hydraulic conductivity, the saturated permeability k was required. The permeability is found from the conductivity by:

$$k = \frac{K\mu}{\rho g} \qquad (5\text{-}3)$$

which is derived from Eq. 2-2. After the generation of the layer information, two pieces of data had to be found on a multilayer level. These are the capillary pressure gradient dp_c/dz and the secondary capillary pressure gradient d^2p_c/dz^2. The capillary pressure gradient was found from the S vs p_c curve with the given pressure assumed to be at the center of each layer. A curve was then drawn through the points to form the depth z vs p_c curve. Tangents were then drawn along the z vs p_c curve to find the dp_c/dz values at different depths. From this data a curve of the dp_c/dz vs z curve was drawn. The values of dp_c/dz were read straight from the curve. The d^2p_c/dz^2 values were found by drawing tangents to the dp_c/dz curve at the depths of the layer centers.

After all the needed data were collected for each of the layers, it was a matter of putting the numbers into the equations reported in Chapter 3. The velocities generated from the equations were then compared to the velocities from the field data. The field velocities were determined by dividing the length of travel for the tritium tracer by the time between samples.

Chapter 6

RESULTS AND COMPARISONS*

To review the contents of the previous chapters, four equations suggested for movement of water through unsaturated soils are compared in this chapter. These are equations of Darcy, Gelhar, Klute, and Morel-Seytoux. Each of these equations requires the use of a relationship between conductivity and water content. There are five such relationships selected for comparison also, namely, those of Averjanov, Corey, Irmay, Laliberte (and Brooks and Corey, referred to as LBC in this report), and Mualem. The former group of equations will be referred to as the velocity equations and the latter group as the conductivity equations. Results obtained from the suggested equations will be compared to a set of unsaturated flow data collected independently at Clemson University by Ligon and Wilson (1972) and Ligon, et al (1980), referred to as the data. Also, in the figures presented in this chapter, reference to other authors is made in the following abbreviated form: mu = Mualem; co = Corey; aver = Averjanov; ir = Irmay; lbc = Laliberte, Brooks and Corey; morel = Morel-Seytoux.

The data are in the form of time of travel of a front of radioactive water through layers of soil from a depth of 110 inches to a depth of 310 inches. The velocity equations were used to generate the same type of information, and plotted as shown in Figs. 6-1 to 6-3. Figure 6-1 shows the prediction of Gelhar's equation of time of travel of water to the given depth. The five conductivity equations are compared as a secondary parameter. The data are also plotted as a reference for the comparisons. Figures 6-2 and 6-3 show similar plots for Morel-Seytoux and Darcy equations. The equation of Klute gives negative values of velocity at some of the layers, and this makes it impossible to compare that equation to the data because the time of travel of water through some layers becomes infinite. It is obvious from the figures that all the velocity equations predict a faster flow velocity for the upper layers of soil (drier, less compacted) and a slower velocity for the deeper layers (wetter, more compacted). Specifically notable is the extremely slow velocities resulting from the use of LBC conductivity equation. It would be a hasty decision at this point to judge that this equation is inadequate for producing good results. However, because the entire time scale of Figs. 6-1 to 6-3 is distorted due to the use of LBC equation, a second set of figures was produced, eliminating the results of LBC beyond the depth of 220 inches. The results are shown in Figs. 6-4 to 6-6. On the expanded time scale of Figs. 6-4 to 6-6 it becomes clear that LBC equation actually produces better results than the other conductivity equations up to a depth of 220 inches for all of the velocity equations. Furthermore, quick eye-judgment would indicate Gelhar equation to work better than the others for predicting flow velocity. This again may be a hasty judgment. To compare the velocity equations side by side, a different set of figures were prepared with the conductivity equations as the main parameter and the velocity equations as the secondary parameter.

*The original figures of this report are in color, but legended such that they can be easily understood in black and white. For the interested reader, color copies can be provided at the cost of $1.00 per page.

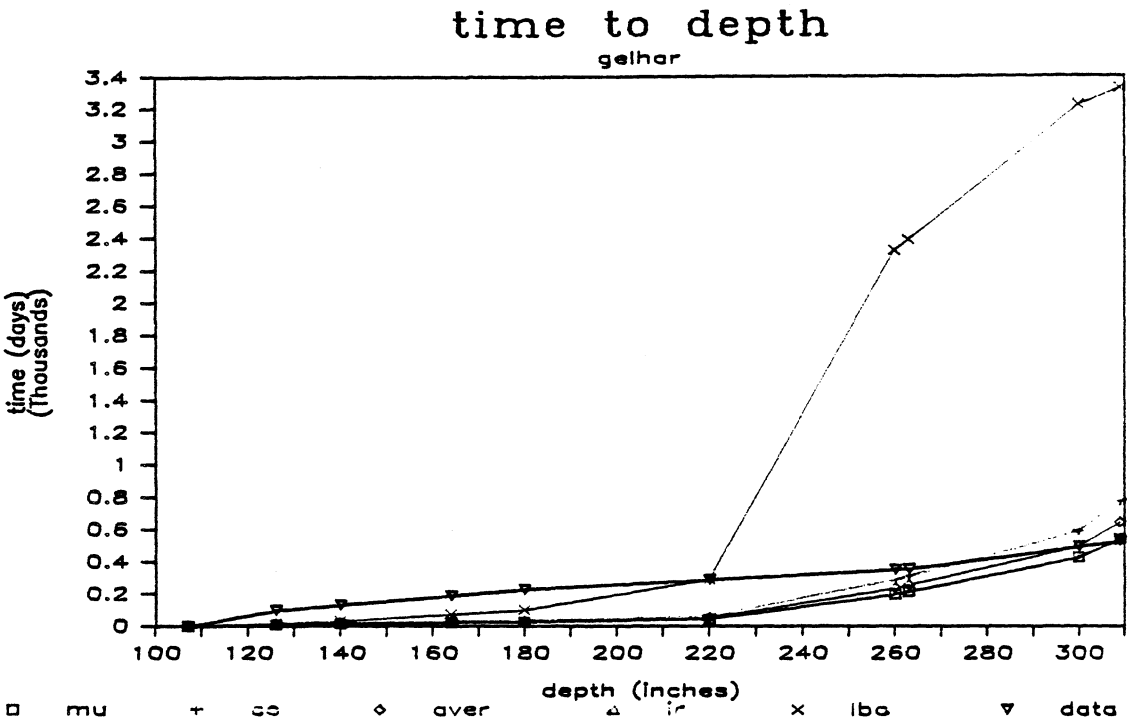

Figure 6-1. Time of Flow to Given Depth by Gelhar Equation

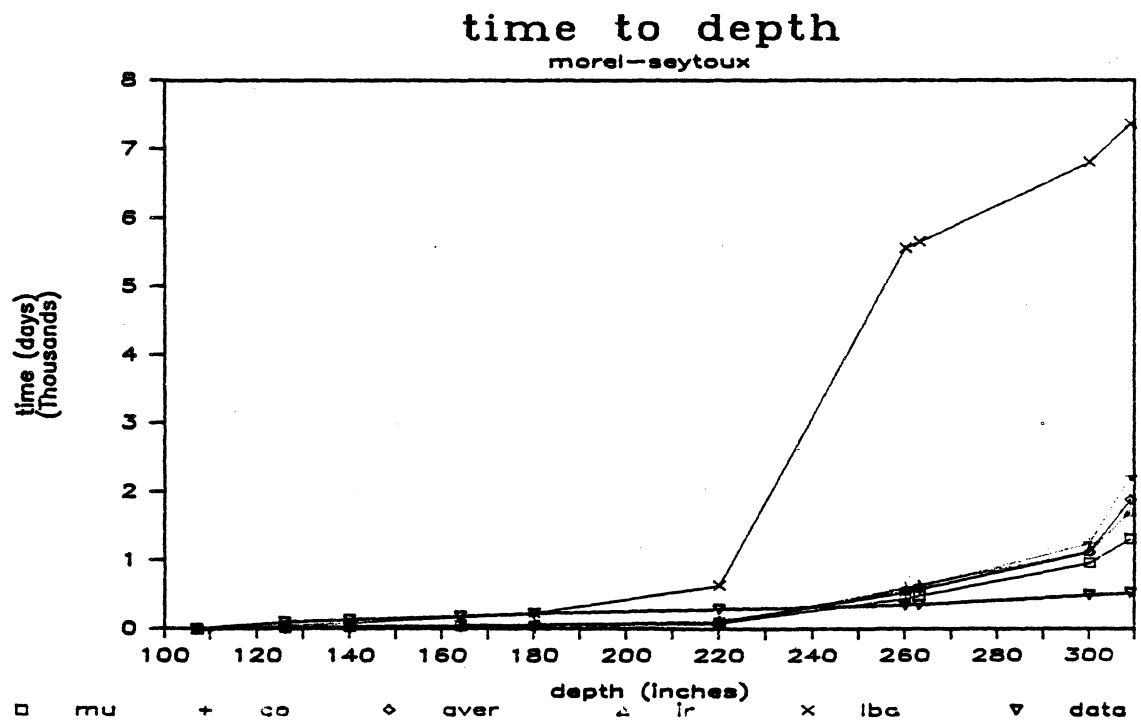

Figure 6-2. Time of Flow to Given Depth by Morel-Seytoux Equation

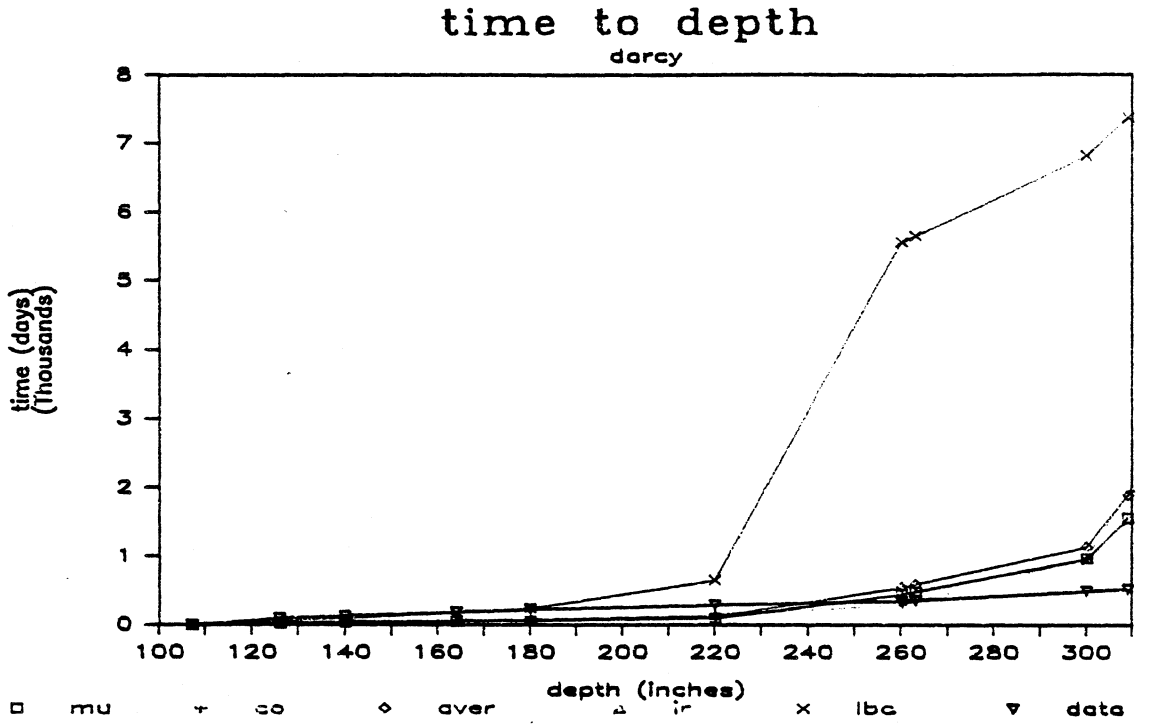

Figure 6-3. Time of Flow to Given Depth by Darcy Equation

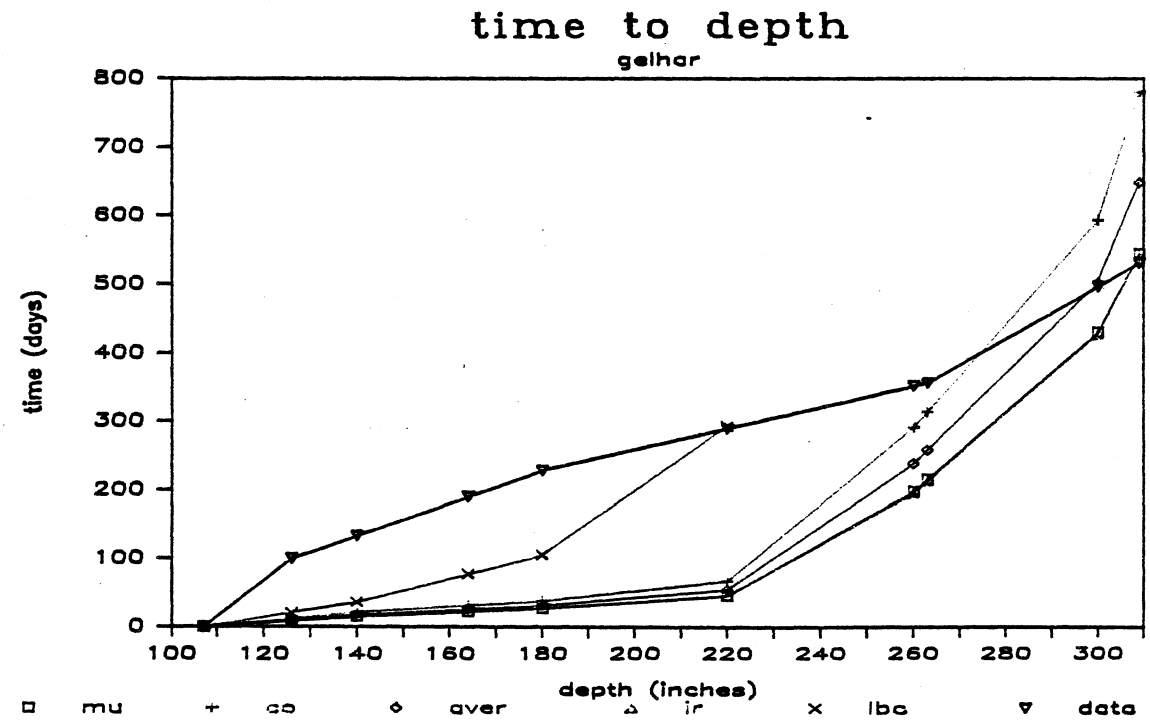

Figure 6-4. Modified Time of Flow vs. Depth by Gelhar Equation

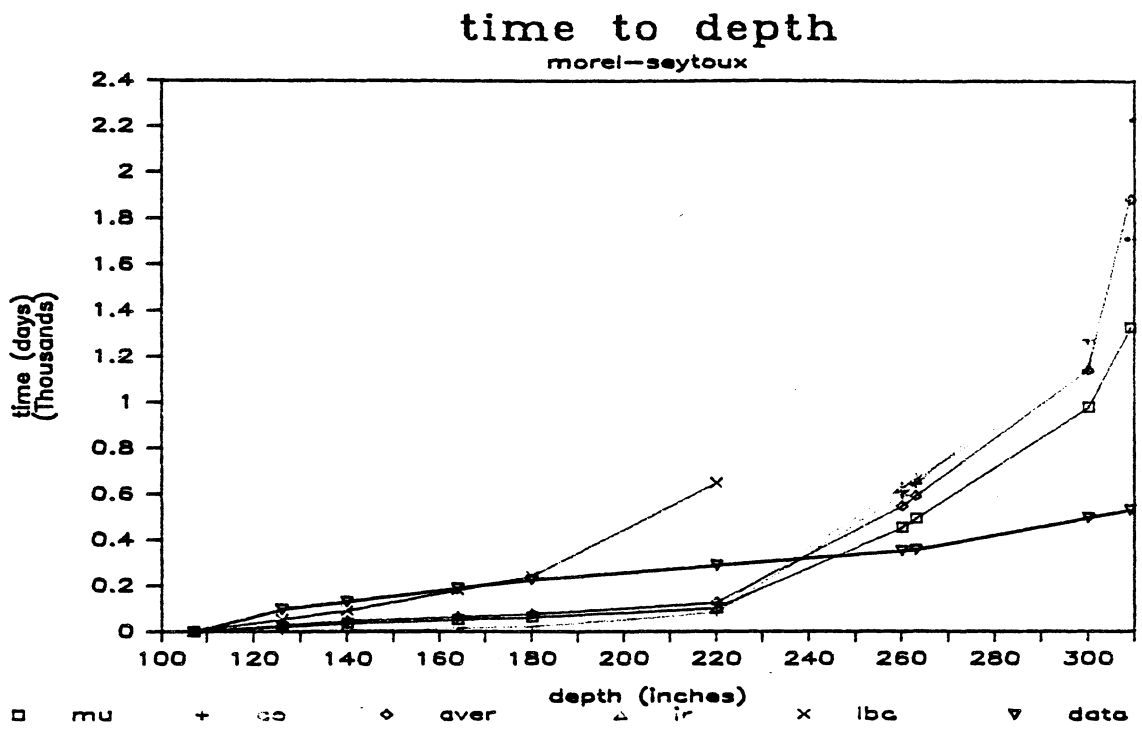

Figure 6-5. Modified Time of Flow vs. Depth by Morel-Seytoux Equation

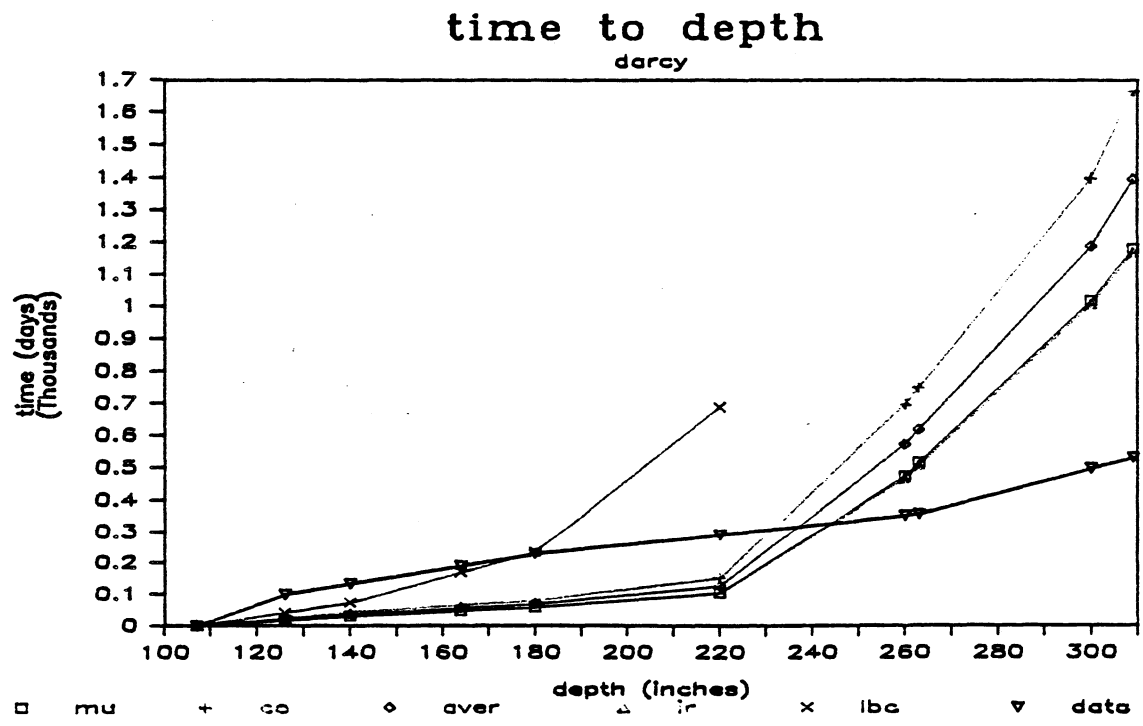

Figure 6-6. Modified Time of Flow vs. Depth by Darcy Equation

The field data are also plotted for comparison. Figure 6-7 shows the flow time to the given depth predicted by all the velocity equations using Mualem conductivity equation. Figures 6-8 to 6-11 are similar plots using Irmay, Averjanov, Corey and LBC equations respectively. The figures are ordered according to largest value on the time scale. Since the total travel time for the field data is a constant for all the figures, the highest value on the time scale of each figure may be thought of as a crude indicator of how well each conductivity equation is performing. Comparison of Figs. 6-7 to 6-10 with Fig. 6-11 indicates one more time that although the LBC equations falls last on the basis of overall travel time, it actually produces better results by any of the velocity equations up to a depth of 220 inches. Comparison of the velocity equations reveals that the equations of Morel-Seytoux and Darcy give very close results, and they are better predictors of velocity to a depth of 220 inches (drier, less compacted soils), while the equation of Gelhar performs better and its results become more parallel to the plot of the field data at the lower depths (wetter, more compacted soils). One point to note is that in the lower depths, where equations of Morel-Seytoux and Darcy predict a travel time of 2000 days for the actual data time of 600 days, the error of prediction is a factor of about 3.5. On the other hand, at the depth of 200 inches where the equation of Gelhar predicts a travel time of 40 days for an actual field time of 300 days, the error of prediction is a factor of 7.5. Therefore, further analysis is necessary before a valid conclusion is reached about which of the suggested equations would be a better predictor of actual flow velocity through unsaturated soils.

To further analyze the equations under study, it was decided to non-dimensionalize the results of the different equations and compare them on a non-dimensional basis. Depth was non-dimensionalized by dividing the depth of each layer by the total profile depth of 310 inches. Velocity was non-dimensionalized by dividing the predicted velocities by the velocities measured for each layer in the field data. The results thus obtained are again compared in two different categories. In the first category, the velocity equations are used as the primary parameter and the conductivity equations as the secondary parameter. Figure 6-12 shows the non-dimensional plot of the results of Darcy equation using the different conductivity equations. The field data show as a line through the non-dimensional velocity of unity. Figures 6-13 to 6-15 show similar results by the equations of Gelhar, Morel-Seytoux and Klute, respectively. There is a single value of velocity for each layer of soil, resulting in a step-wise plot as shown.

The figures are ordered according to the highest value on the non-dimensional velocity scale. This time the equation of Klute can be included in the comparison, despite the fact that it sometimes predicts negative velocities, meaning that there would be no downward flow at some layers of soil. This result is contrary to the data. It is interesting to note that where the equation of Klute produces positive velocities, its results are good. It is also noteworthy that the combination of the velocity equation of Morel-Seytoux with the conductivity equation of Corey is a poor one and without it the equation of Morel-Seytoux would give very good results.

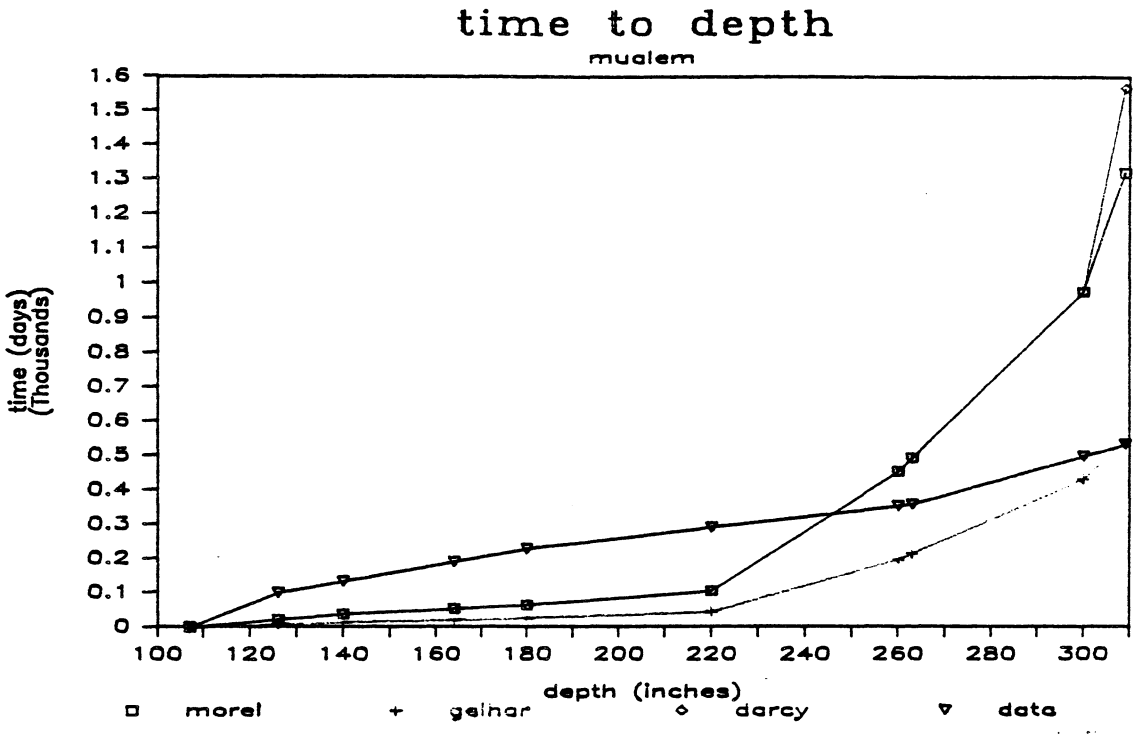

Figure 6-7. Time of Flow vs. Depth Using Mualem Equation

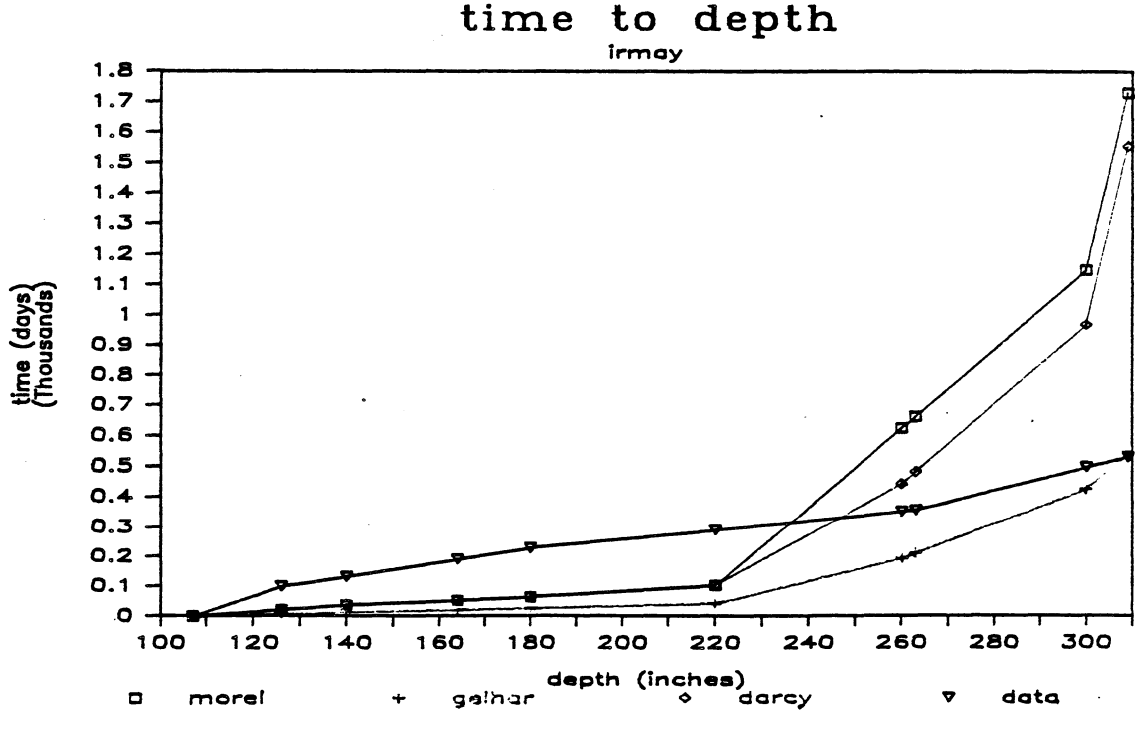

Figure 6-8. Time of Flow vs. Depth Using Irmay Equation

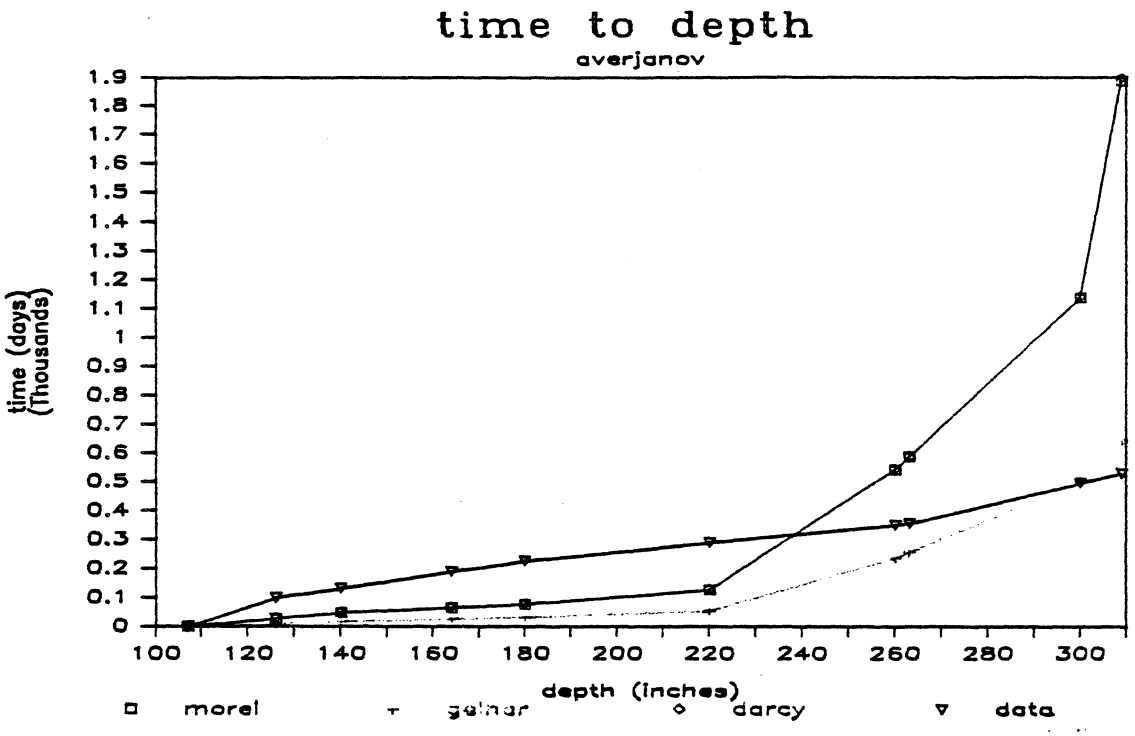

Figure 6-9. Time of Flow vs. Depth Using Averjanov Equation

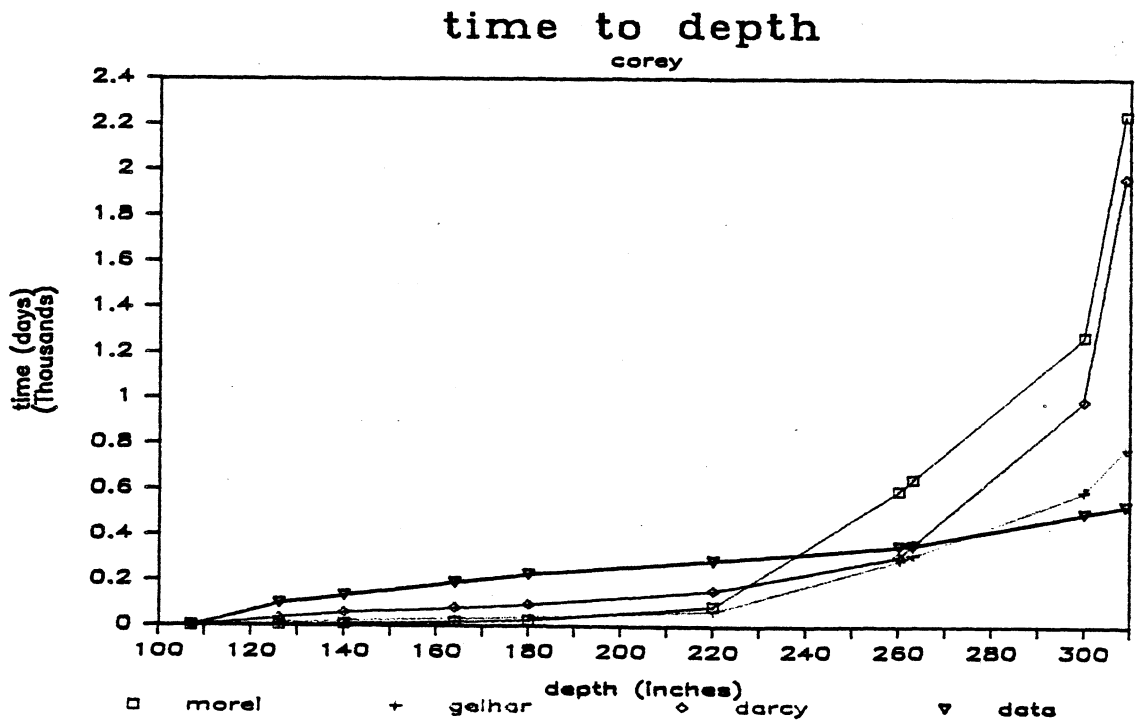

Figure 6-10. Time of Flow vs. Depth Using Corey Equation

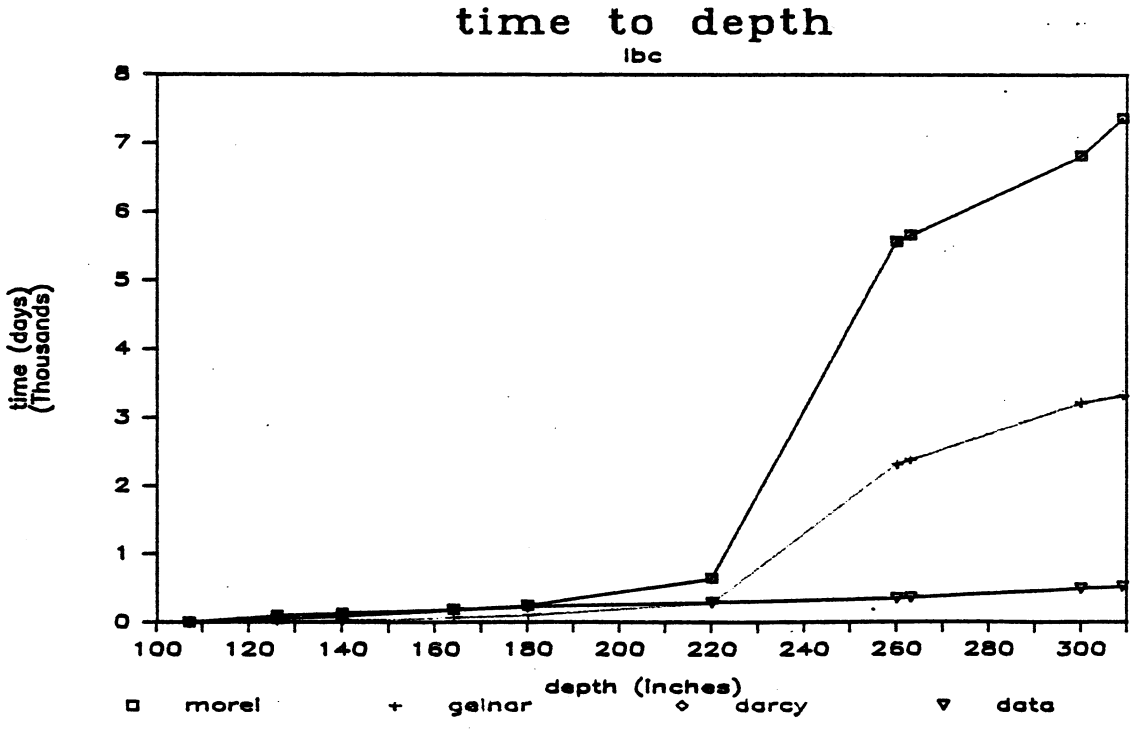

Figure 6-11. Time of Flow vs. Depth Using LBC Equation

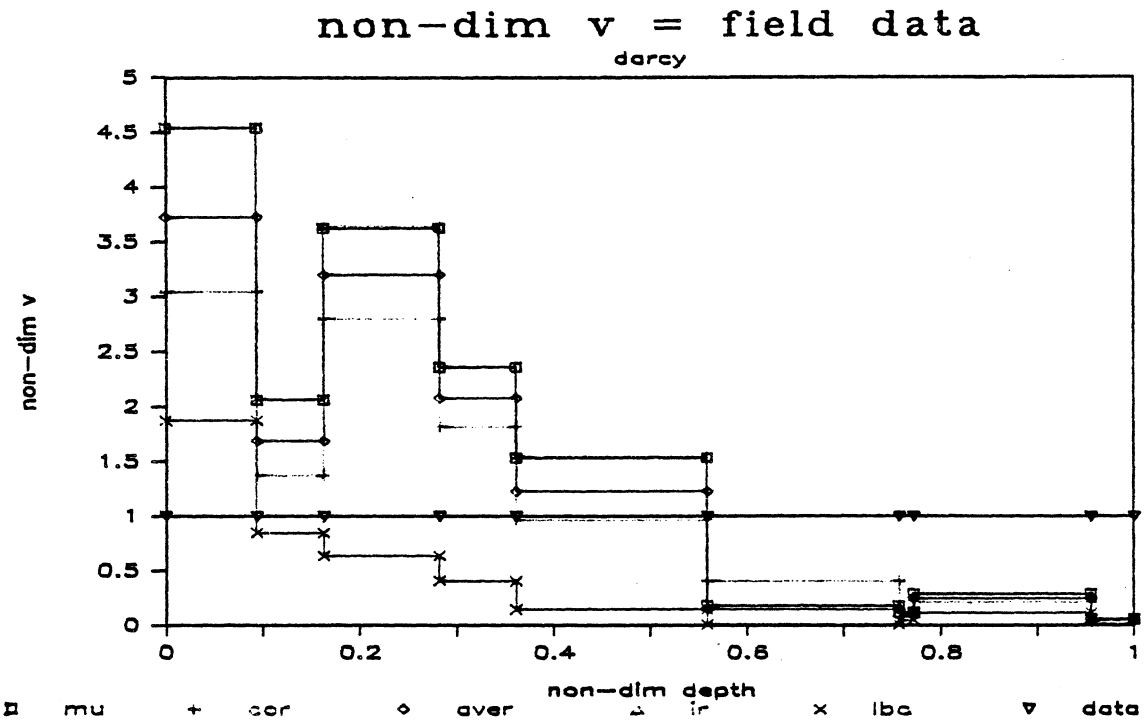

Figure 6-12. Plot of Velocity vs. Depth by Darcy Equation, Non-Dimensionalized by Field Data

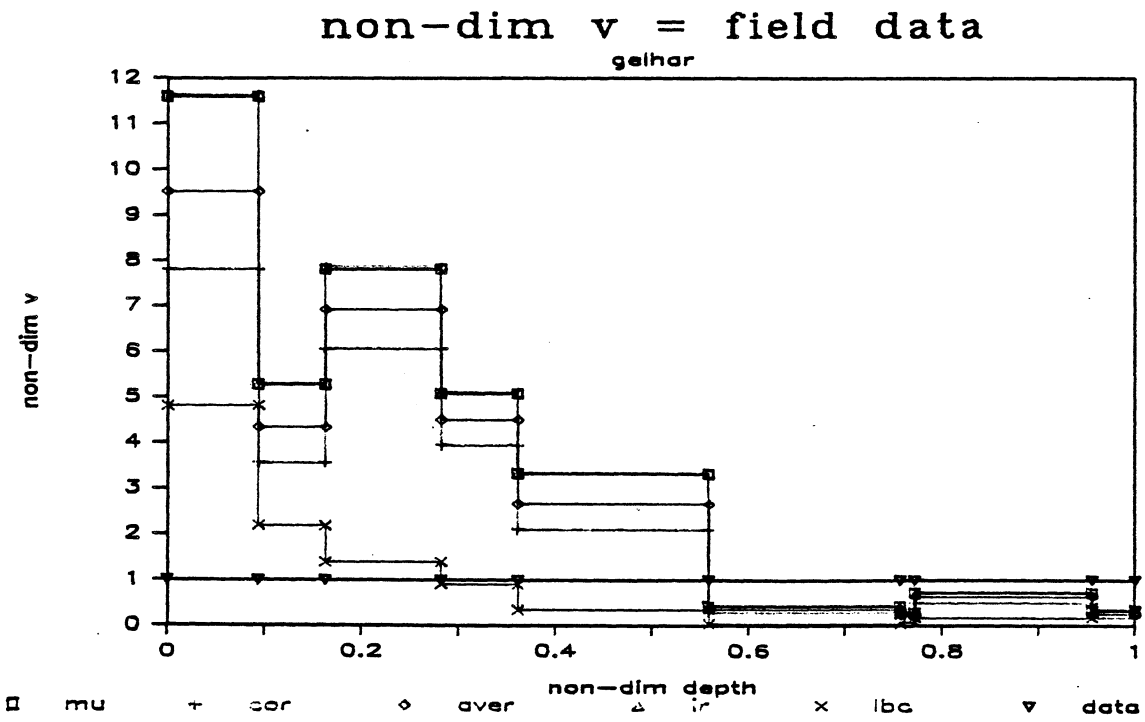

Figure 6-13. Plot of Velocity vs. Depth by Gelhar Equation, Non-Dimensionalized by Field Data

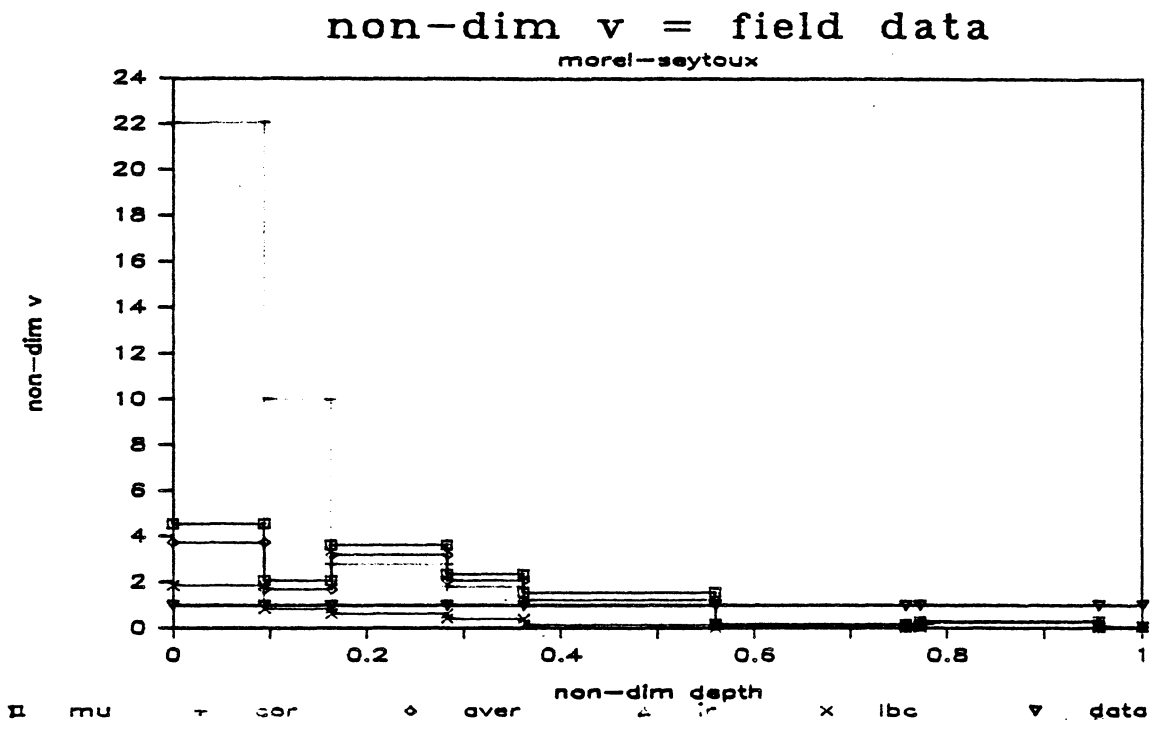

Figure 6-14. Plot of Velocity vs. Depth by Morel-Seytoux Equation, Non-Dimensionalized by Field Data

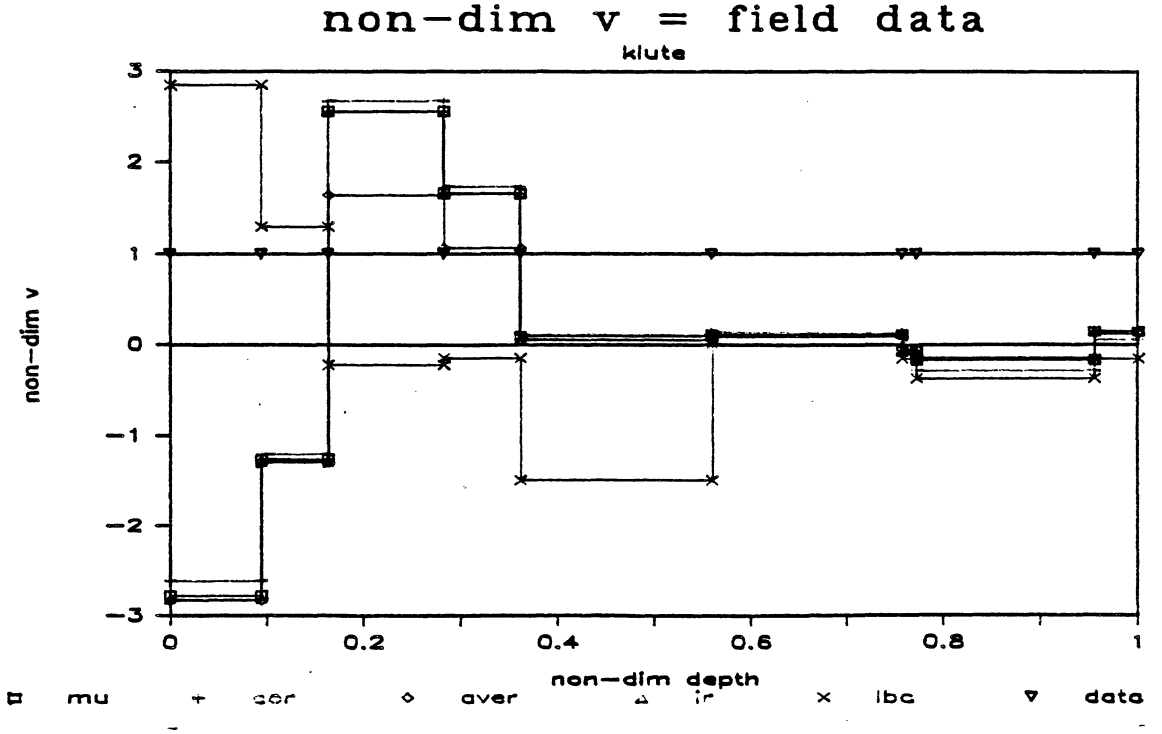

Figure 6-15. Plot of Velocity vs. Depth by Klute Equation, Non-Dimensionalized by Field Data

A second category of dimensionless plots are prepared by plotting the velocity equations side by side as shown in Figs. 6-16 to 6-20. The conductivity equations are the primary parameters between the figures. Again, the line representing the field data is a straight line through the dimensionless velocity of unity. The closer the predicted velocity of an equation to this line, the better is its prediction. The figures are one more time ordered according to the highest value on the dimensionless velocity scale. It is interesting to note that the conductivity equation of LBC seems to be clearly a more suitable equation for any of the velocity equations, including the negative values of Klute equation. Visual inspection of Figs. 6-16 to 6-20 indicates that the equations of Morel-Seytoux and Darcy produce results that are similar and close to field data, the combination of Morel-Seytoux and Darcy once again being the exception.

Visual comparison can be misleading in certain situations. For a better comparison of such similar plots as Figs. 6-16 to 6-20 it is preferable to obtain a numerical indicator of the closeness of the predictions to the filed data. To determine such a numerical indicator, calculations of root mean square of the data of Figs. 6-16 to 6-20 were made, as shown in Table 6-1. This will give a relatively simple yet an indicative parameter for comparison of the different equations. Comparison of the columns shows a clear advantage for the LBC equation. Comparison of the rows reveals the extremely similar results of the equations of Darcy and Morel-Seytoux, excepting the poor combination of Morel-Seytoux equation with that of Corey, which had been noticed before. Either equation seems adequate for predicting flow velocities. However, in view of the more comprehensive coverage of the factors involved in motion of liquids through porous media, the equation of Morel-Seytoux in combination with LBC is recommended. Contaminants may not always be transported in the form of small quantities of dissolved materials in water, they may be fluids such as jet fuel, which require a more detailed consideration of factors involved than Darcy equation utilizes.

Table 6-1. Root Mean Squares of the Predicted Dimensionless Velocities*

Equation	Averjanov	Corey	Irmay	LBC	Mualem
Darcy	16.98	11.37	25.85	5.54	25.30
Gelhar	134.81	90.30	202.59	19.39	199.42
Klute	25.19	26.43	27.44	17.95	27.14
Morel-Seytoux	16.99	532.35	25.85	5.69	25.47

*Root Mean Square = Σ (predicted v - Data v)^2 over different layers

Consideration of Table 6-1 shows small values of the root mean square for Klute equation. This equation is considered accurate by the authors and the reason it gives negative values of velocity is that it uses the differences in hydraulic conductivity between layers. When a less permeable layer overlies a more permeable layer, as flow becomes unsaturated the capillary pressure in the top layer becomes higher than the lower layer and flow stops. Whereas this analysis is true of heavy soils overlying light soils, in a continuous and gradually changing column of solid such as the one used for collection of the field data it may not apply. Failure of Klute equation in this case is because of

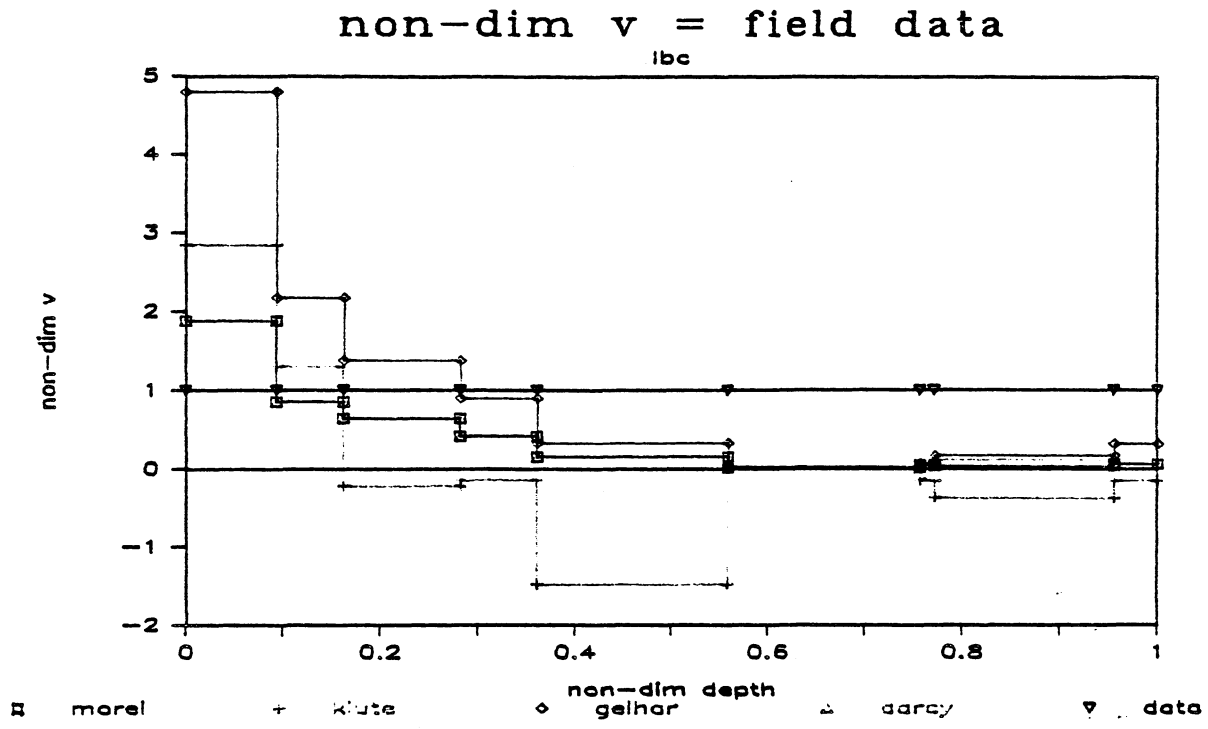

Figure 6-16. Non-Dimensional Plot of Velocity vs. Depth Using LBC Equation Based on the Field Data

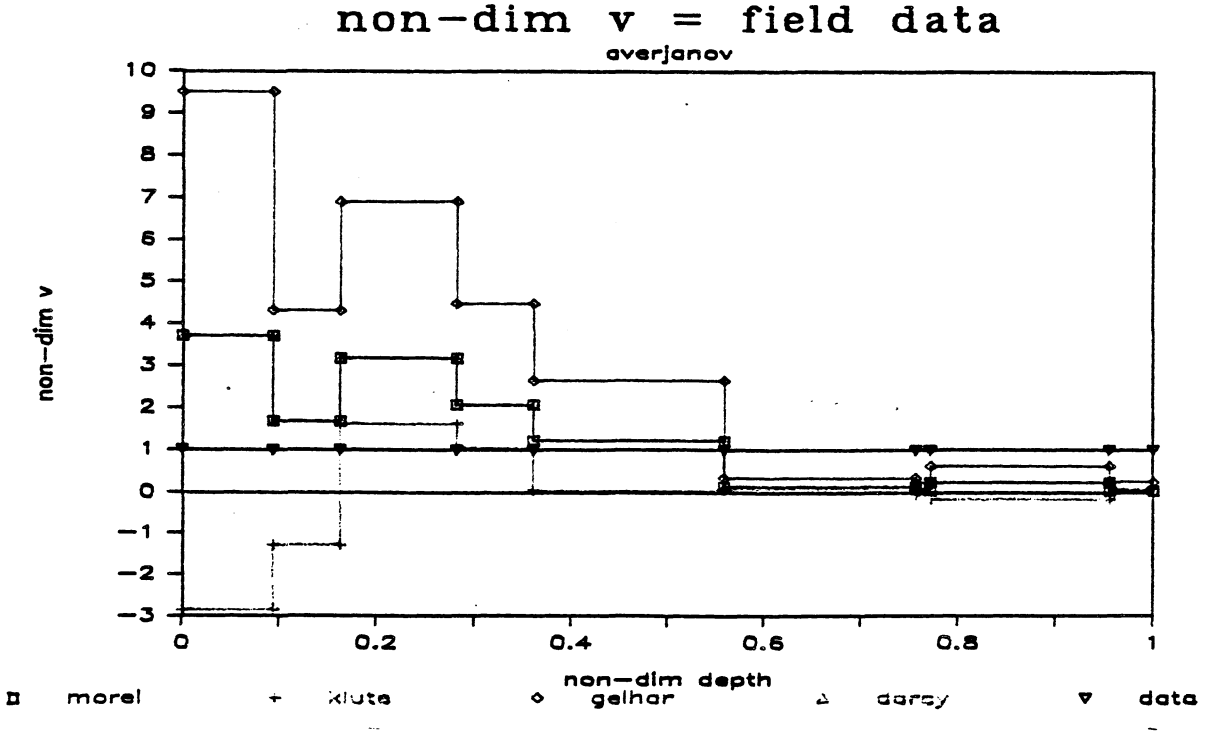

Figure 6-17. Non-Dimensional Plot of Velocity vs. Depth Using Averjanov Equation Based on the Field Data

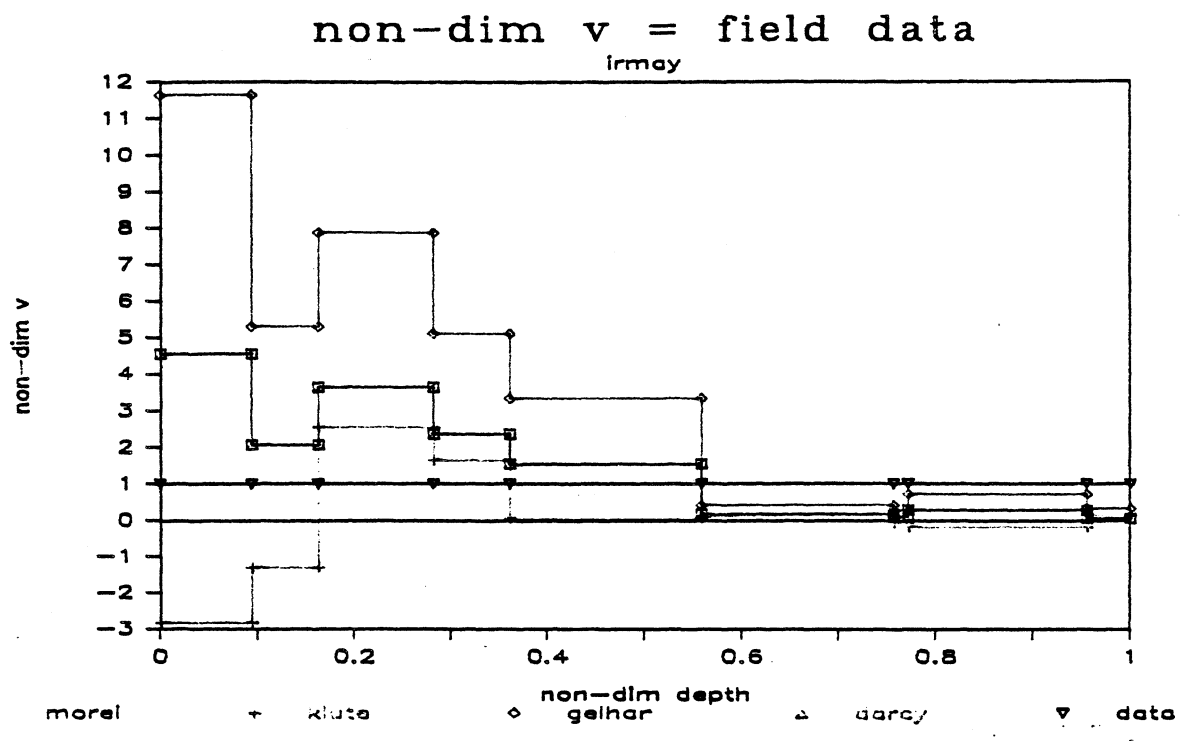

Figure 6-18. Non-Dimensional Plot of Velocity vs. Depth Using Irmay Equation Based on the Field Data

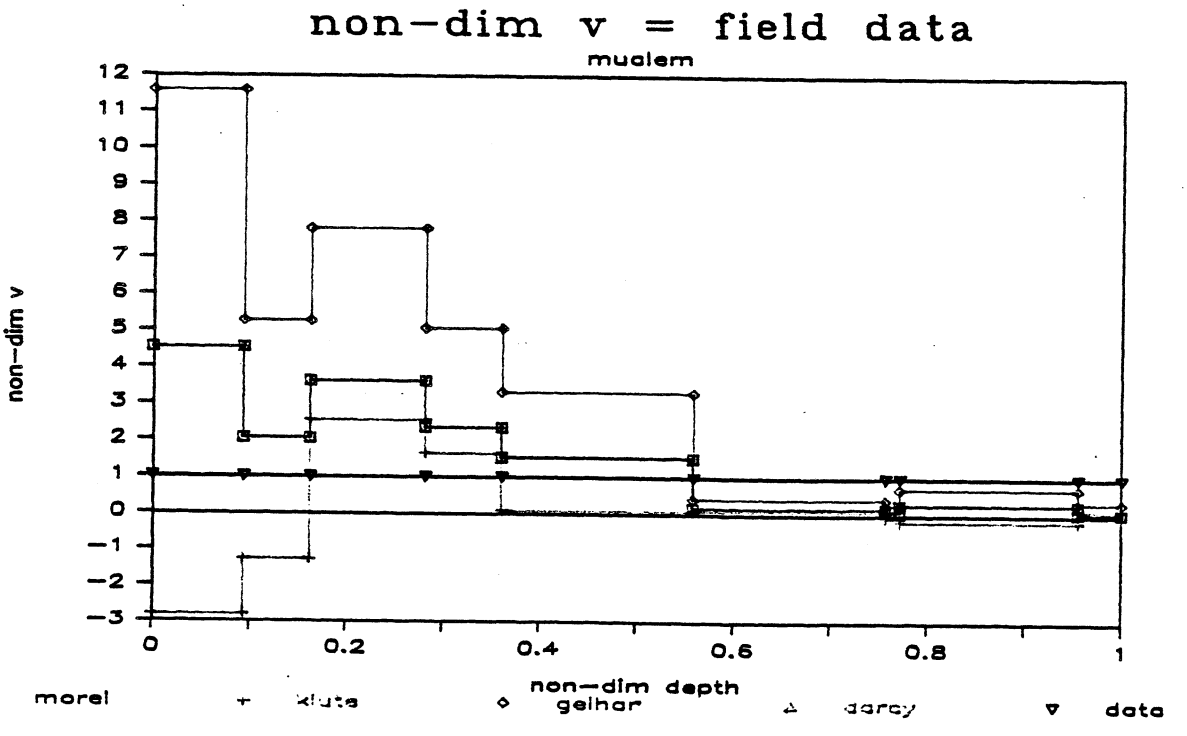

Figure 6-19. Non-Dimensional Plot of Velocity vs. Depth Using Mualem Equation Based on the Field Data

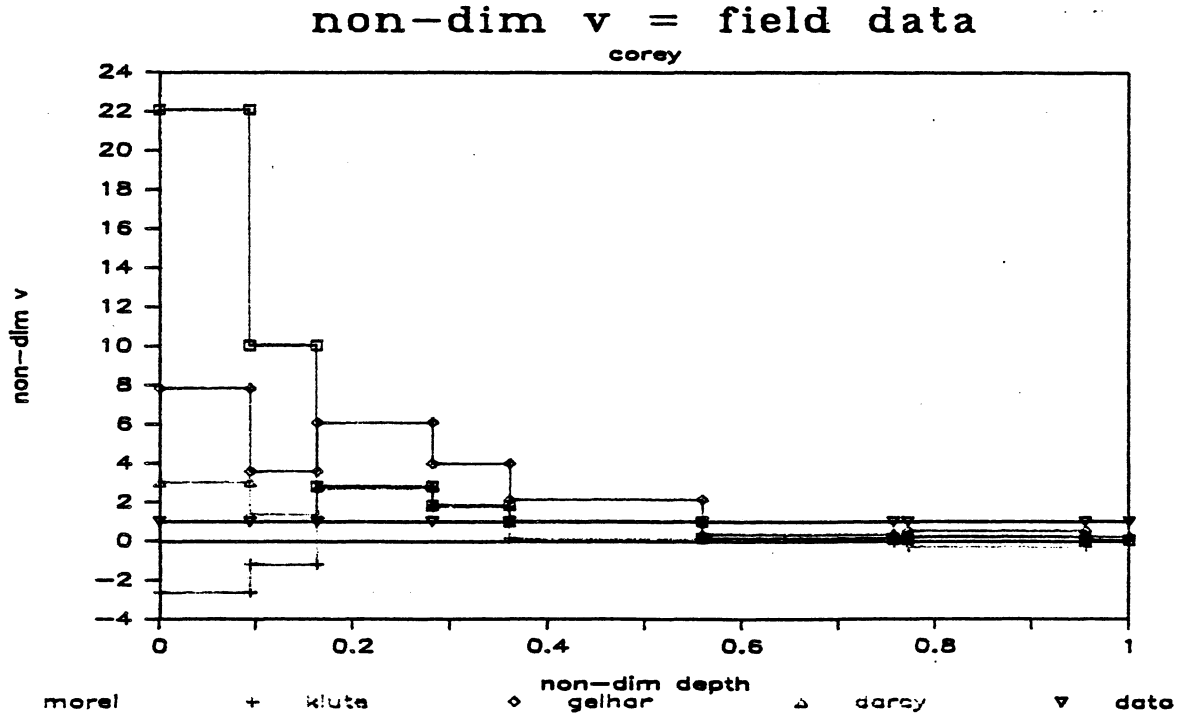

Figure 6-20. Non-Dimensional Plot of Velocity vs. Depth Using Corey Equation Based on the Field Data

discretizing the properties of a continuous medium. The negative velocities are not acceptable in this case, and therefore the equation of Klute was eliminated from Figs. 6-16 to 6-20 and the figures were replotted in Figs. 6-21 to 6-25. The values of Table 6-1 can be visually verified by comparing these figures.

Careful observation of all the figures shows that there is a consistent deviation of the equations from the field data at lower depths. The field data were collected by sampling water at different intervals of time until the radioactive water front passed the sampling site. Because of such a consistent deviation of all the suggested velocity equations from the field data, it was suspected that actually the field data may have somehow been in error in the lower depths. To test this hypothesis a set of figures was prepared where velocities were non-dimensionalized using the velocity equation of Morel-Seytoux and the conductivity equation of LBC. Figure 6-26 shows a non-dimensionalized plot of velocity vs depth based on the Morel-Seytoux - LBC combination for the Morel-Seytoux equation itself. Naturally, the line for LBC would be a straight line through non-dimensional velocity of unity. The largest difference observed is 18-fold of the base equation. If the field data are included in the plot, as shown in Fig. 6-27, the difference between the base equation and the field data becomes 100-fold. Figures 6-28 to 6-30 show similar plots using other velocity equations side by side. Figures 6-31 to 6-35 have been prepared which are self-explanatory. The equation of Klute has been eliminated from this set to avoid negative velocities. The root mean squares for the last set of plots were calculated for comparison, as shown in Table 6-2. Values in this table are higher than the values in Table 6-1, indicating that with this combination, the variability within the velocity equations is more than the variability between the equations and the field data. It is worth noting that in this method of calculations the differences are squared and hence differences are exaggerated. The very high value of the root mean square for the data is indicative of the disagreement of the data as shown in Figs. 6-25 to 6-35. This analysis does not decisively eliminate the possibility of errors in the field data for the lower layers of the soil profile. But it does indicate that overall, the equations under study agree with the field data better than they agree amongst themselves for the tested combinations.

Table 6-2. Root Mean Squares of the Non-Dimensionalized Velocity Equations on the Basis of the Morel-Seytoux-LBC Combination.

Equation	Averjanov	Corey	Irmay	LBC	Mualem
Darcy	335	215	501	9	497
Gelhar	2000	1319	2927	54	2897
Klute	119	343	204	328	182
Morel-Seytoux	336	447	501	0	499

In further attempts to analyze the performance of the equations under study, it was decided to quantify the order of magnitude of the errors of velocity prediction by the different equations. The graphs presented thus far contain an important factor that is not readily obvious to the viewer. It has been discussed before, that on the non-dimensional plots the field data represent a straight line at the

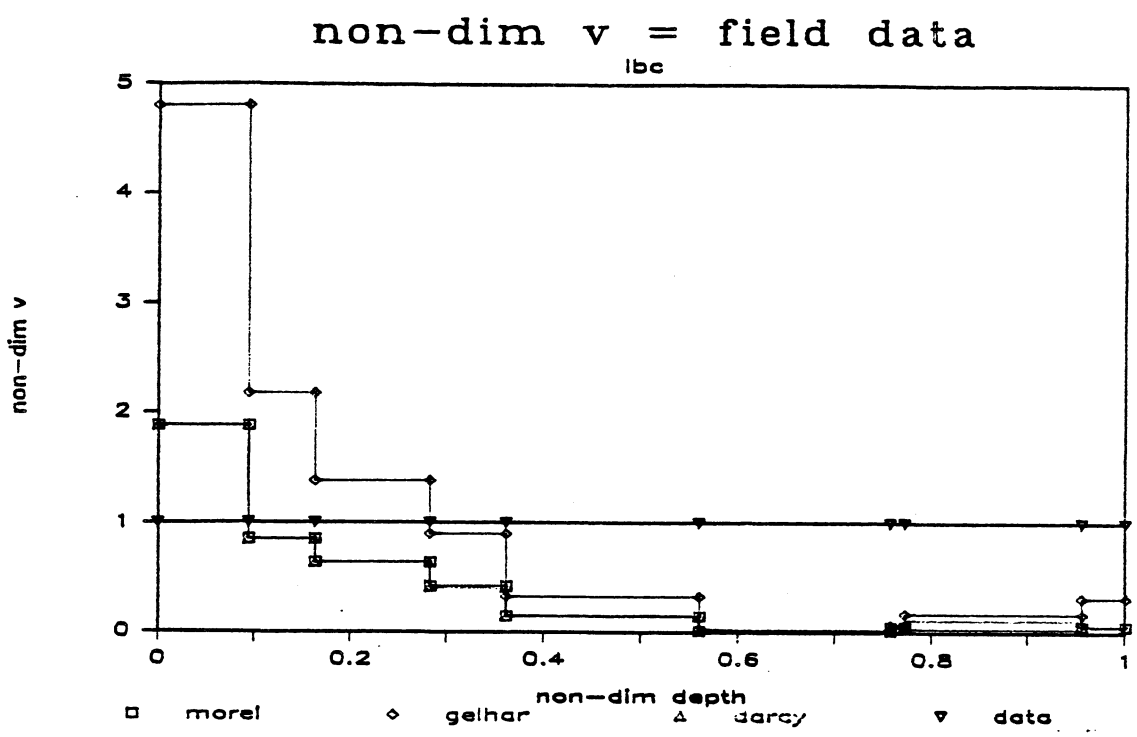

Figure 6-21. Non-Dimensional Plot of the Positive Velocity Equations Based on the Field Data Using LBC Equation

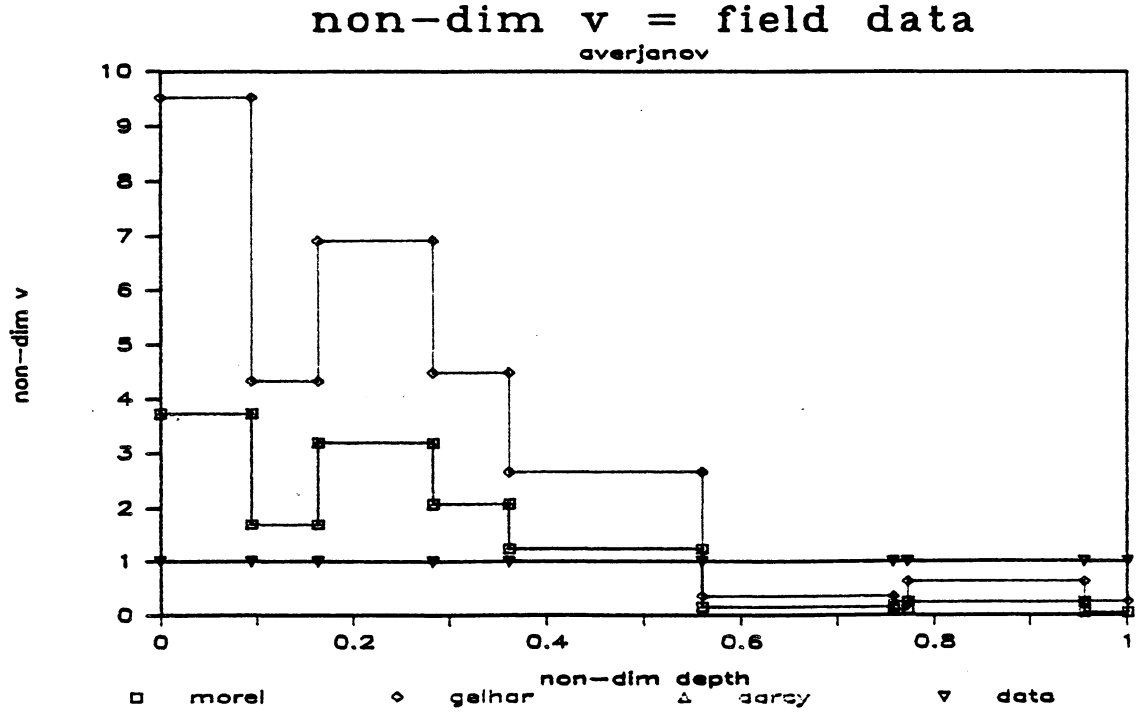

Figure 6-22. Non-Dimensional Plot of the Positive Velocity Equations Based on the Field Data Using Averjanov Equation

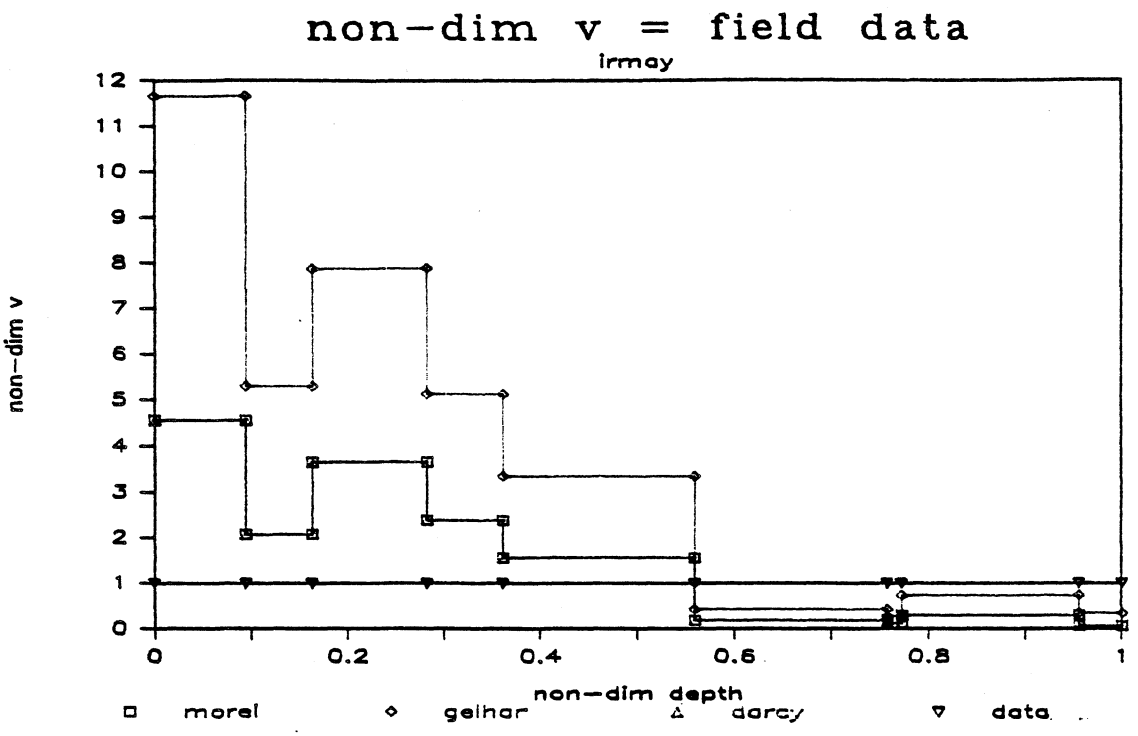

Figure 6-23. Non-Dimensional Plot of the Positive Velocity Equations Based on the Field Data Using Irmay Equation

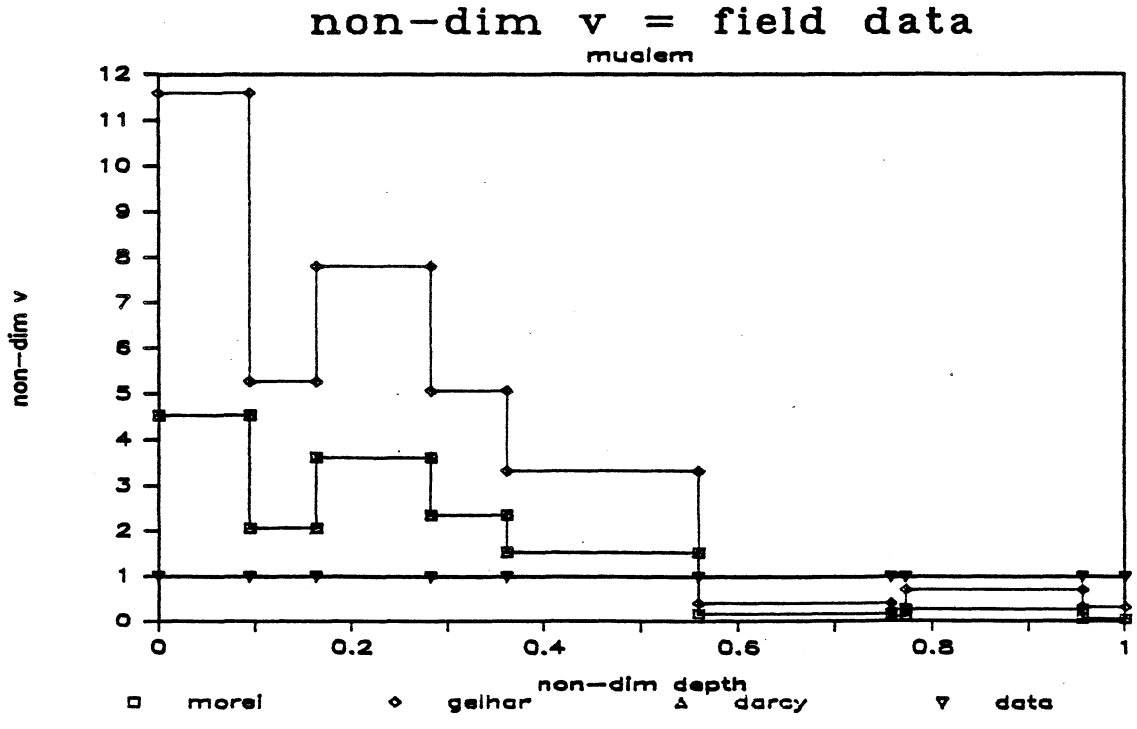

Figure 6-24. Non-Dimensional Plot of the Positive Velocity Equations Based on the Field Data Using Mualem Equation

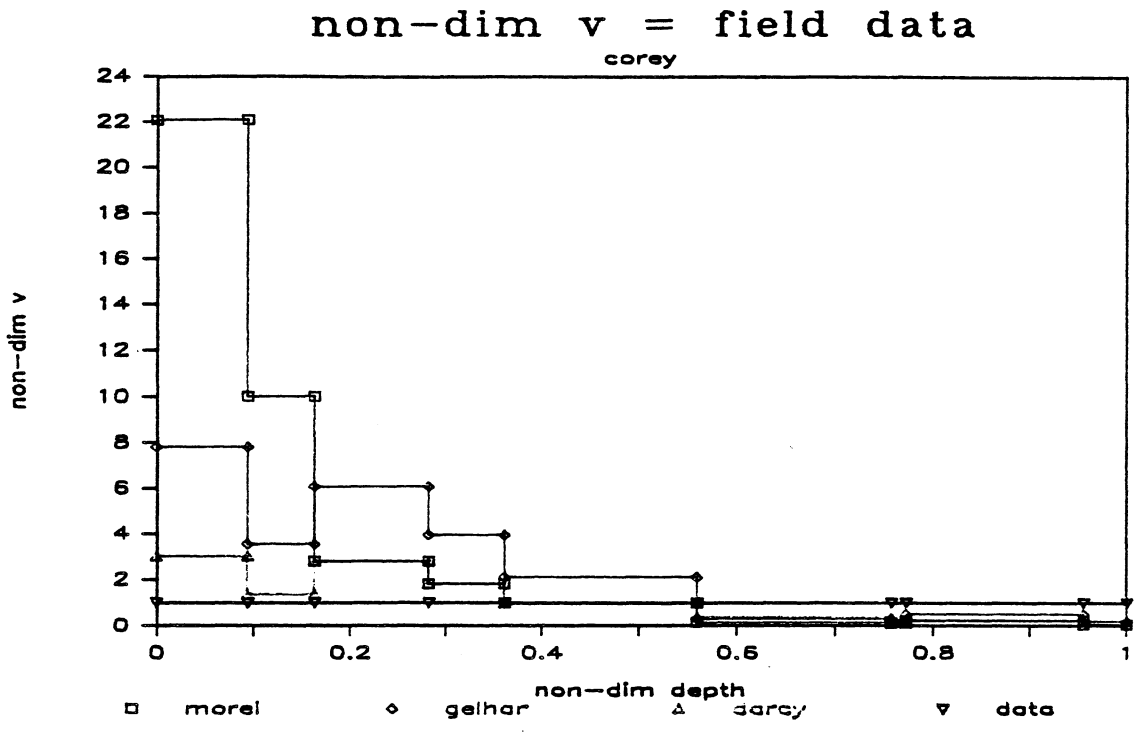

Figure 6-25. Non-Dimensional Plot of the Positive Velocity Equations Based on the Field Data Using Corey Equation

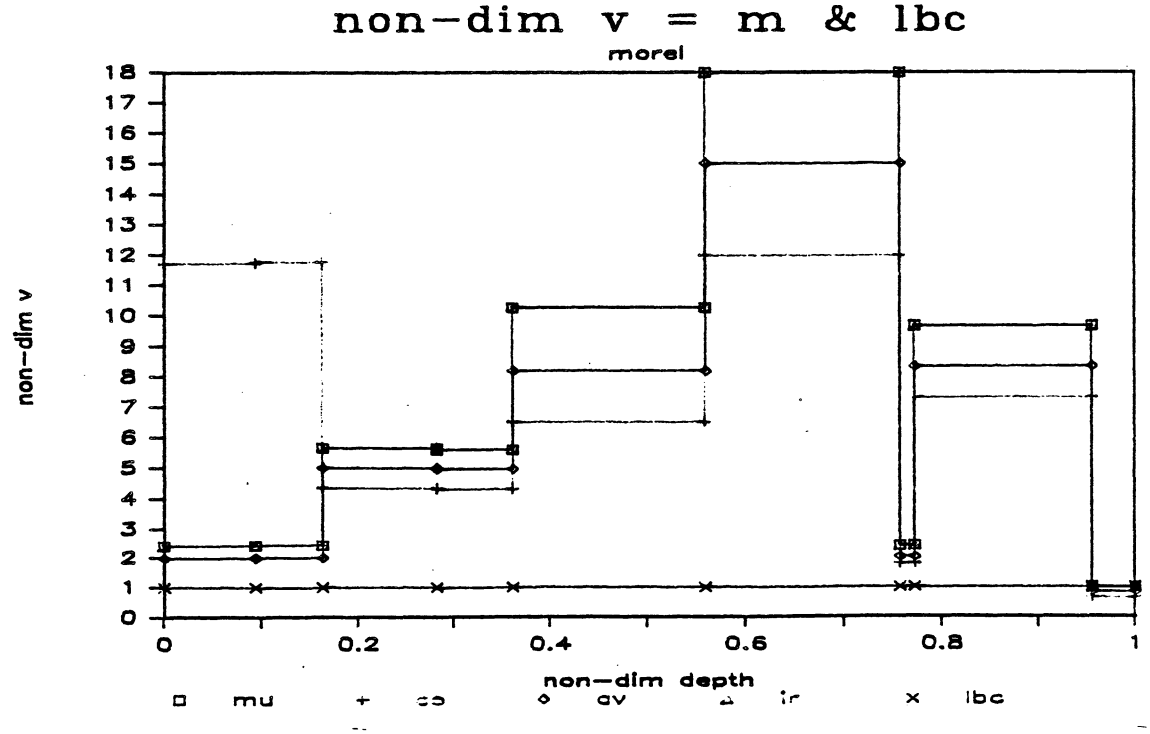

Figure 6-26. Non-Dimensional Plot of Morel-Seytoux Equation Based on Morel-Seytoux-LBC Combination

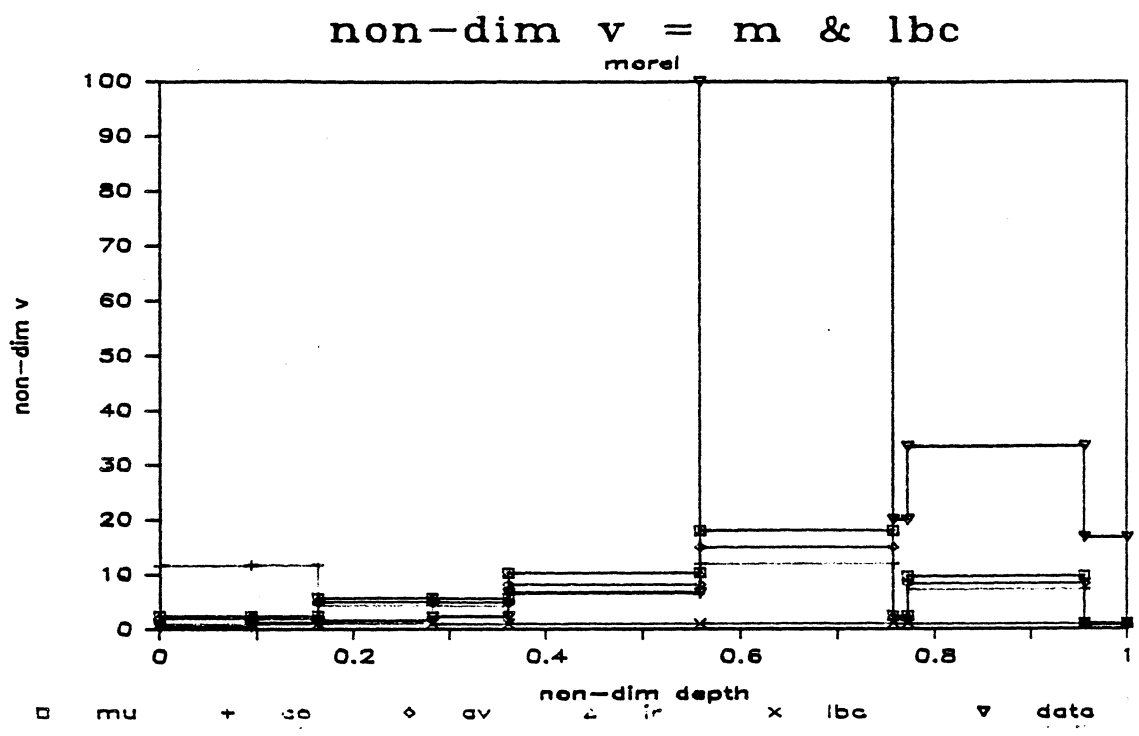

Figure 6-27. Non-Dimensional Plot of Morel-Seytoux Equation Based on Morel-Seytoux-LBC Combination Including the Field Data

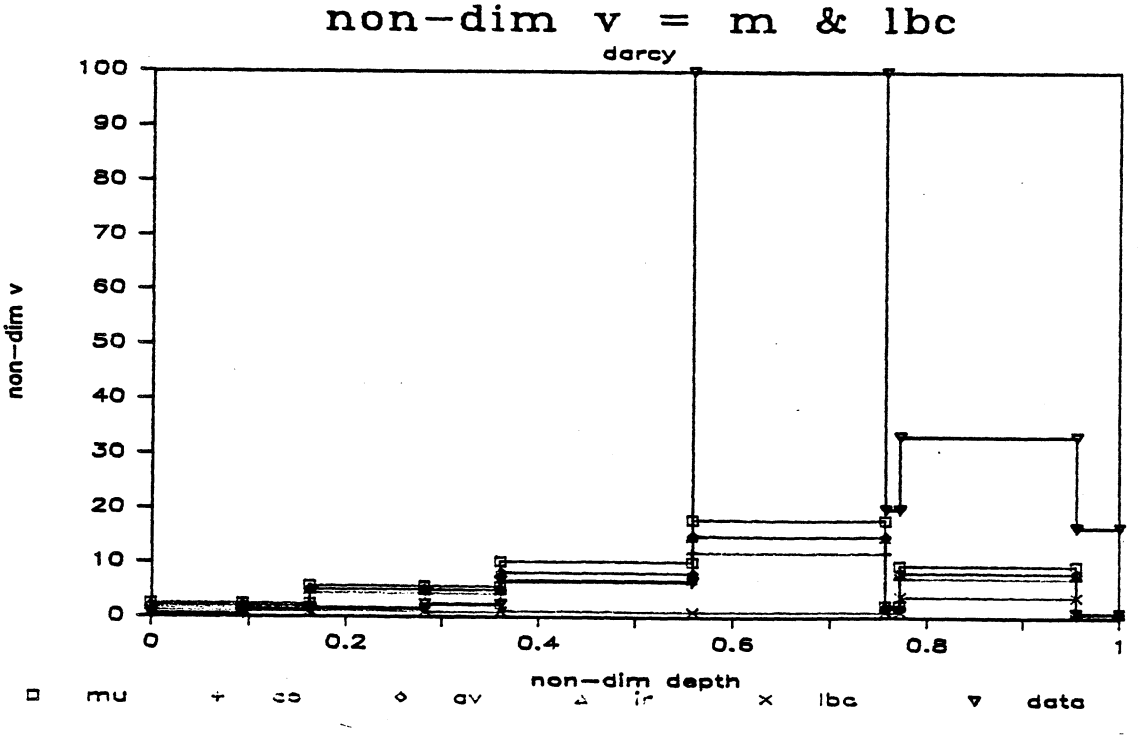

Figure 6-28. Non-Dimensional Plot of Darcy Equation Based on Morel-Seytoux-LBC Combination Including the Field Data

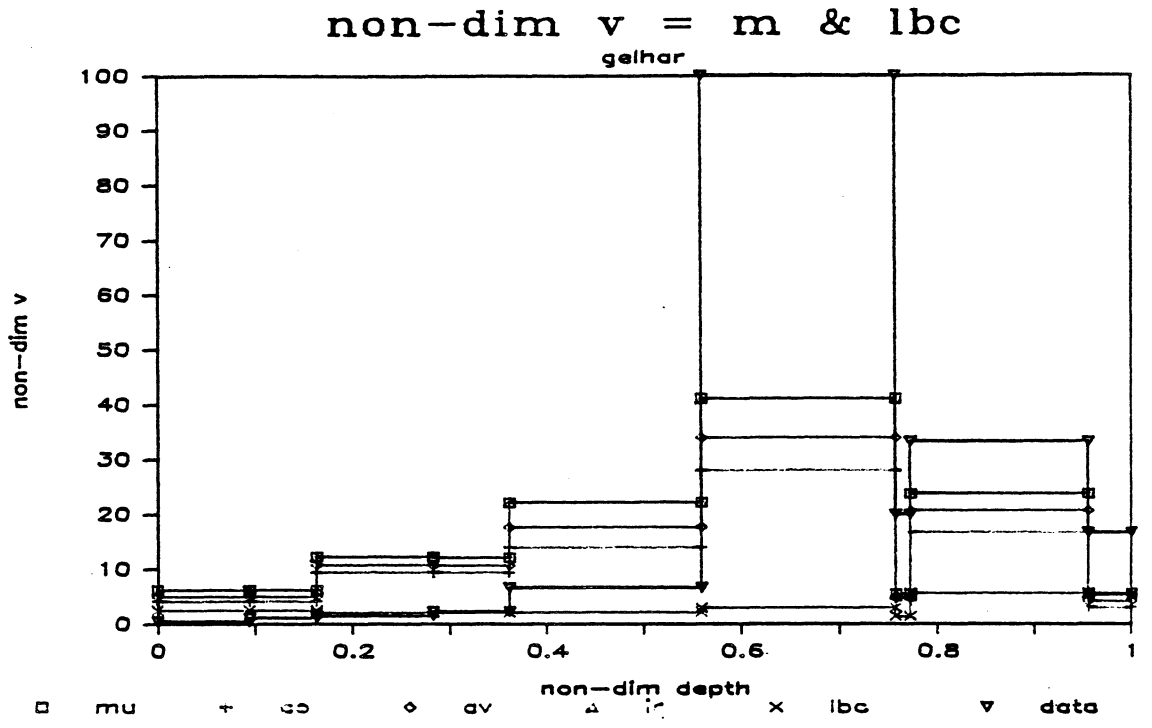

Figure 6-29. Non-Dimensional Plot of Gelhar Equation Based on Morel-Seytoux-LBC Combination Including the Field Data

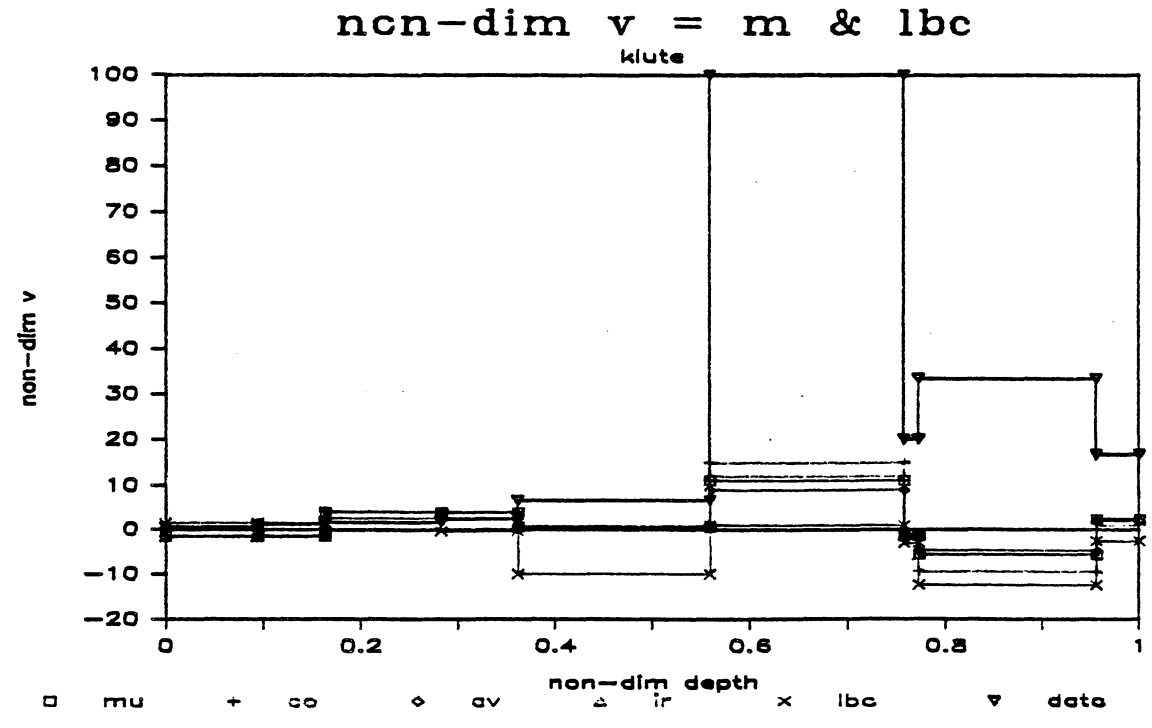

Figure 6-30. Non-Dimensional Plot of Klute Equation Based on Morel-Seytoux-LBC Combination Including the Field Data

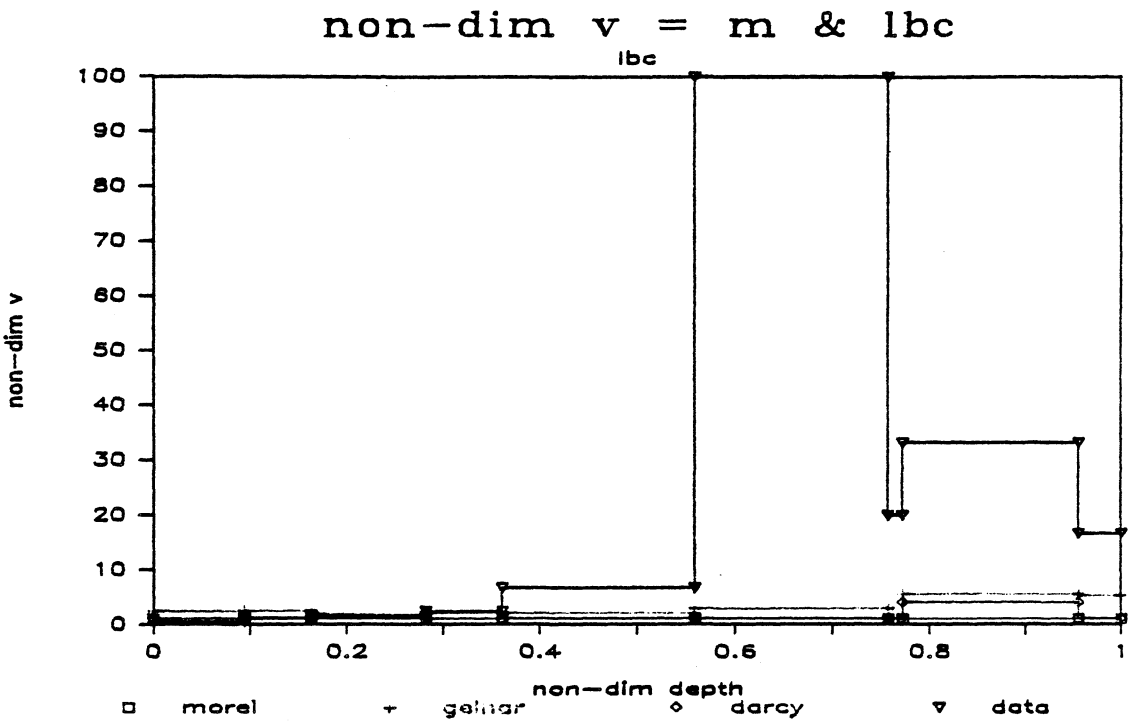

Figure 6-31. Non-Dimensional Plot of Velocity vs. Depth Based on the Morel-Seytoux-LBC Combination Using the LBC Equation

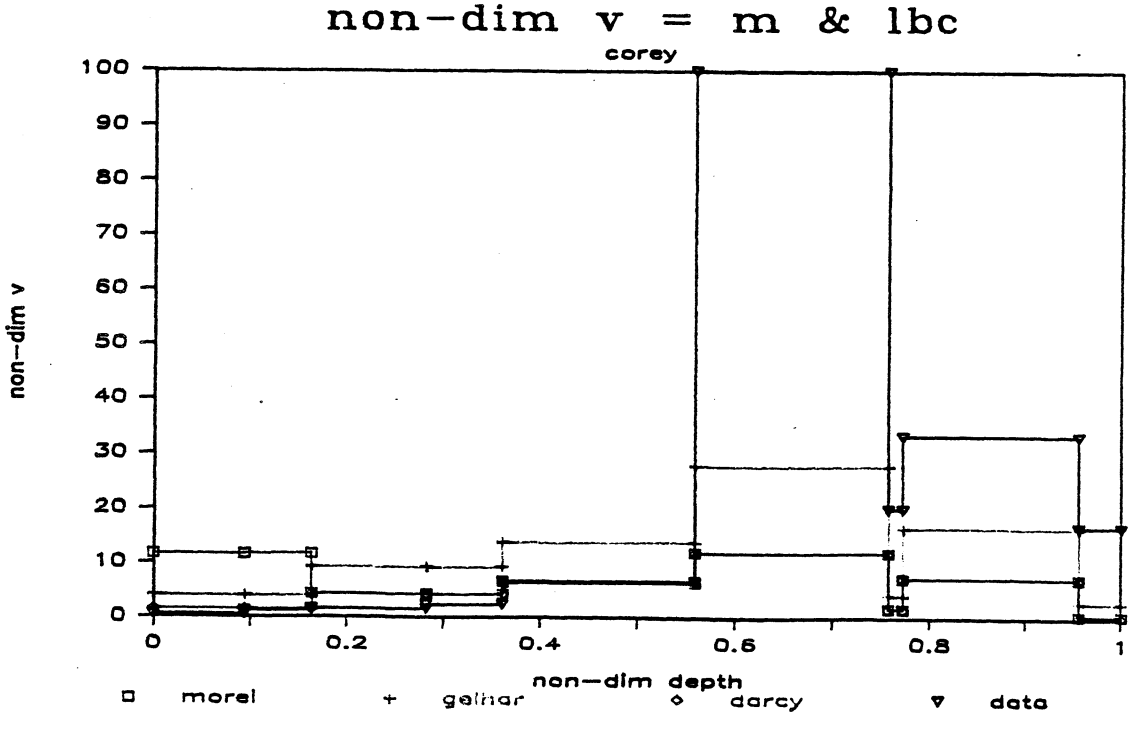

Figure 6-32. Non-Dimensional Plot of Velocity vs. Depth Based on the Morel-Seytoux-LBC Combination Using the Corey Equation

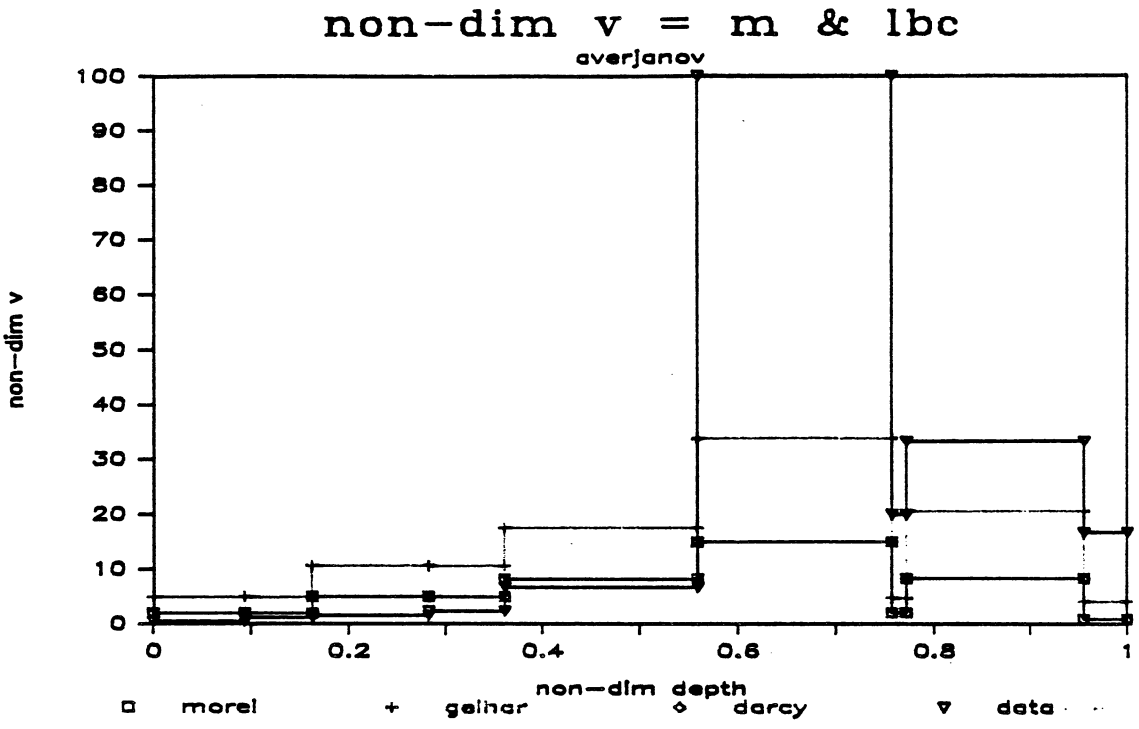

Figure 6-33. Non-Dimensional Plot of Velocity vs. Depth Based on the Morel-Seytoux-LBC Combination Using the Averjanov Equation

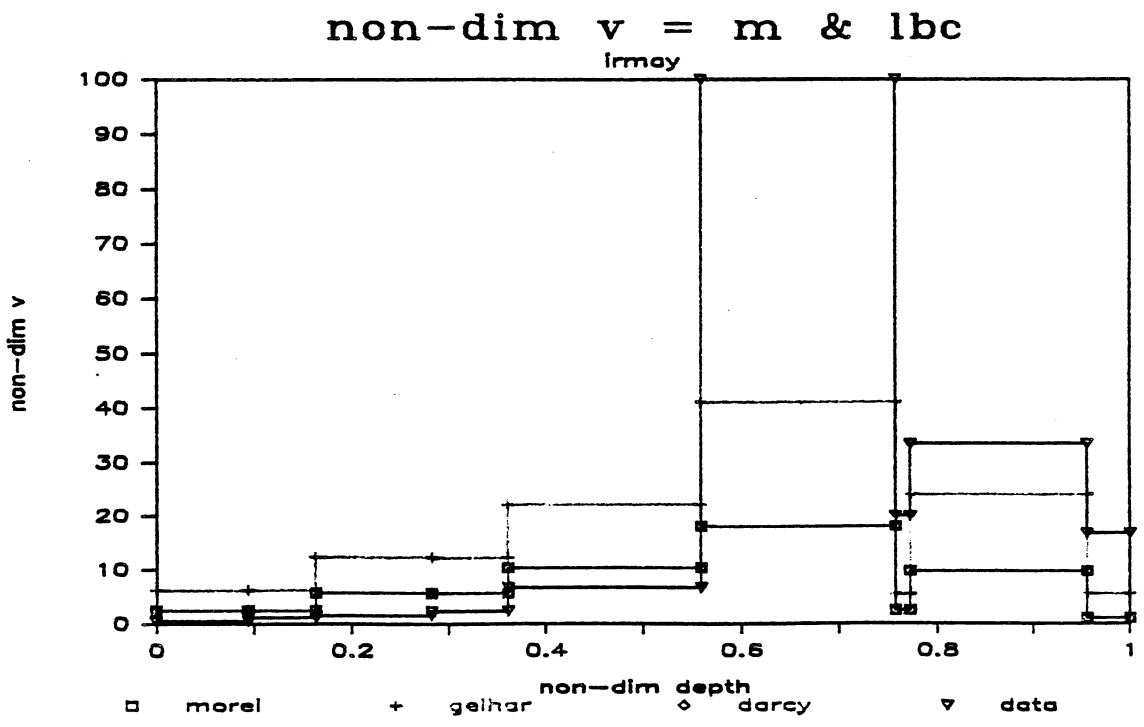

Figure 34. Non-Dimensional Plot of Velocity vs. Depth Based on the Morel-Seytoux-LBC Combination Using the Irmay Equation

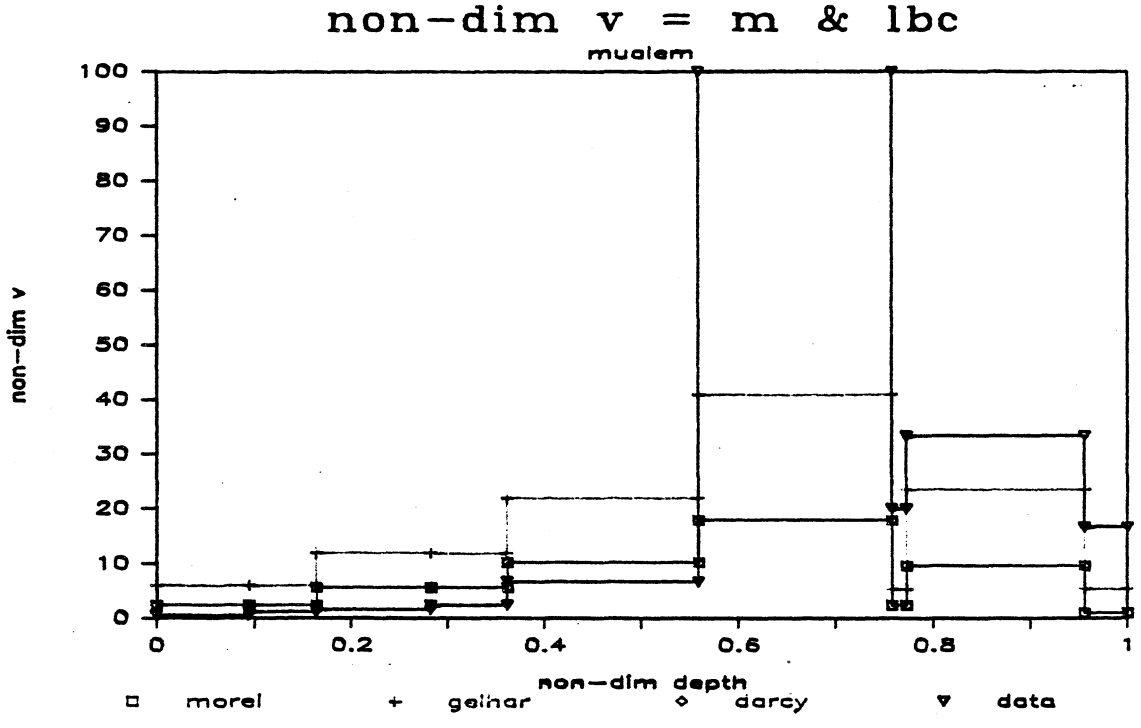

Figure 6-35. Non-Dimensional Plot of Velocity vs. Depth Based on the Morel-Seytoux-LBC Combination Using the Mualem Equation

non-dimensional velocity of unity. Above this line, the velocity equations may predict velocities of up to four fold. Below the line (and above the axis where velocity is zero) the velocity equations may predict velocities of 1/10 to 1/50 of the field data, which is off by more than an order of magnitude. These two errors should not be given equal weight. In order to quantify how the velocity equations perform with respect to errors of one or two orders of magnitude, root mean square calculations were performed on the logarithms of the non-dimensionalized velocities. The results are summarized in Table 6-3. The equation of Klute was not included in the analysis because the logarithm of a negative number is undefined. Table 6-3 indicates that the equation of LBC gives the worst and that of Corey gives the best results of this analysis. Examination of the rows shows that the equation of Gelhar is producing better results by this analysis. This result does not contradict the earlier finding that the equation of Morel-Seytoux with LBC gives better results. The fact is that these two equations are suited to two different conditions. To the extent of being able to verify against the existing set of field data, for less compacted soils, on the dry side of the moisture content curve, the equation of Morel-Seytoux with that of LBC is a better predictor of flow velocity through the soil. On the other hand, for more compacted soils with higher moisture contents, the equation of Gelhar combined with the conductivity equation of Corey can be expected to give better results.

Table 6-3. Root Mean Square of Logarithms of Non-Dimensional Velocity Predictions Based on the Field Data

Equation	Averjanov	Corey	Irmay	LBC	Mualem
Darcy	4.48	5.21	4.21	8.98	4.19
Gelhar	3.68	3.58	3.96	5.32	3.94
Morel-Seytoux	4.48	7.20	4.21	10.44	4.20

Chapter 7

CONCLUSIONS AND RECOMMENDATIONS

The equations under study have each been derived for certain conditions for which they may be expected to produce satisfactory results. In this study an effort was made to compare four equations of flow velocity in unsaturated media using an independent set of data that was not tailored to the needs of any of the equations. For this reason, five equations of hydraulic conductivity as a function of moisture content were also used and compared. The analyses presented in Chapter 6 point to two combinations that can be expected to produce results verifiable by the field data of this study. For flow under low moisture content and less compacted soils the equation of Morel-Seytoux combined with the equation of Laliberte, Brooks and Corey produced the best results. For more compacted soils under higher moisture content, the equation of Gelhar combined with the equation of Corey produced better results than other combinations. The knowledge of the capabilities of these equations is extremely important and at times critical for predicting the fate of a front of contaminant moving under unsaturated conditions in the underground water resources.

The information gained in this study is only a starting point in shedding light on the available methods of predicting the movement of water and other contaminants through soils under unsaturated conditions. Much more extensive work needs to be done in collecting or identifying actual data of movement of water in unsaturated soils in order to delineate and define the range of applicability of the existing equations of flow. Modification to the presently existing equations and methodologies may be recommended in order to arrive at a more generally applicable flow equation in unsaturated soils.

Chapter 8

BIBLIOGRAPHY

Averjanov, S.F., 1950, About Permeability of Subsurface Soils in Case of Incomplete Saturation, The Theory of Ground Water Movement, Engineering Collection Volume VII.

Brooks, R.H., Corey A.T., June 1966, Properties of Porous Media Affecting Fluid Flow, Journal of Irrigation and Drainage Division, American Society of Civil Engineers.

Childs, E.C., 1969, Introduction to the Physical Basis of Soil Water Phenomena, John Wiley & Sons Limited, New York.

Corey, A.T., 1977, Mechanics of Heterogenous Fluids in Porous Media, Water Resources Publications, Fort Collins, Colorado.

El-Khatib, N.A.F., December 1980, The Relative Permeabilities of an IdealizedModel of Two-Phase Flow in Porous Media, Applied Mathematical Modeling, Volume 4.

Freeze, R.A. and Cherry, J.A., 1979, Groundwater, Prentice Hall, Inc., England Cliffs, N.J. 07632.

Irmay, S., June 1954, On the Hydraulic Conductivity of Unsaturated Soils, Transactions of the American Geophysical Union, volume 35, Number 3.

Klute, A., 1969, The Movement of Water in Unsaturated Soils, Progress of Hydrology, University of Illinois.

Laliberte, G.E., Brooks, R.H., Corey, A.T., March 1968, Permeability Calculated from Desaturated Data, Journal of Irrigation and Drainage Division, American Society of Civil Engineers.

Ligon, J.T., Wilson, T.V., April 1972, Deep Seepage in Piedmont Watersheds, Water Resources Research Institute, Clemson University, Clemson, South Carolina.

Ligon, J.T., Wilson, T.V., Allen, J.F., King, T.G., Singh, U.P., January 1980, Water Distribution and Movement in an Unsaturated Piedmont Soil Profile, Water Resources Institute, Clemson University, Clemson, South Carolina.

Morel-Seytoux, H.J. 1973, Two-Phase Flow in Porous Media, Volume 9, Academic Press, New York.

Mualem, Y., June 1976, A New Model for Predicting the Hydraulic Conductivity of Unsaturated Porous Media, Water Resources Research, Volume 12, Number 3.

Wilson, J.L., Gelhar, L.W., 1974, Dispersive Mixing in a Partially Saturated Porous Media, Report #191, Ralph M. Parson Laboratory, Massachusetts Institute of Technology.